Assimilation of SSM/I-Derived Surface Rainfall and Total Precipitable Water for Improving the GEOS Analysis for Climate Studies

ARTHUR Y. HOU, DAVID V. LEDVINA,* ARLINDO M. DA SILVA, SARA Q. ZHANG,+ JOANNA JOINER, AND ROBERT M. ATLAS

Data Assimilation Office, Laboratory for Atmospheres, NASA Goddard Space Flight Center, Greenbelt, Maryland

GEORGE J. HUFFMAN# AND CHRISTIAN D. KUMMEROW

Mesoscale Atmospheric Processes Branch, Laboratory for Atmospheres, NASA Goddard Space Flight Center, Greenbelt, Maryland

(Manuscript received 10 August 1998, in final form 30 March 1999)

ABSTRACT

This article describes a variational framework for assimilating the SSM/I-derived surface rain rate and total precipitable water (TPW) and examines their impact on the analysis produced by the Goddard Earth Observing System (GEOS) Data Assimilation System (DAS). The SSM/I observations consist of tropical rain rates retrieved using the Goddard Profiling Algorithm and tropical TPW estimates produced by Wentz.

In a series of assimilation experiments for December 1992, results show that the SSM/I-derived rain rate, despite current uncertainty in its intensity, is better than the model-generated precipitation. Assimilating rainfall data improves cloud distributions and the cloudy-sky radiation, while assimilating TPW data reduces a moisture bias in the lower troposphere to improve the clear-sky radiation. Together, the two data types reduce the monthly mean spatial bias by 46% and the error standard deviation by 26% in the outgoing longwave radiation (OLR) averaged over the Tropics, as compared with the NOAA OLR observation product. The improved cloud distribution, in turn, improves the solar radiation at the surface. There is also evidence that the latent heating change associated with the improved precipitation improves the large-scale circulation in the Tropics. This is inferred from a comparison of the clear-sky brightness temperatures for TIROS Operational Vertical Sounder channel 12 computed from the GEOS analyses with the observed values, suggesting that rainfall assimilation reduces a prevailing moist bias in the upper-tropospheric humidity in the GEOS system through enhanced subsidence between the major convective centers.

This work shows that assimilation of satellite-derived precipitation and TPW can reduce state-dependent systematic errors in the OLR, clouds, surface radiation, and the large-scale circulation in the assimilated dataset. The improved analysis also leads to better short-range forecasts, but the impact is modest compared with improvements in the time-averaged signals in the analysis. The study shows that, in the presence of biases and other errors of the forecast model, it is possible to improve the time-averaged ''climate content'' in the data without comparable improvements in forecast. The full impact of these data types on the analysis cannot be measured solely in terms of forecast skills.

1. Introduction

This study explores the use of satellite-derived rainfall and total precipitable water (TPW) estimates in four-dimensional (4D) data assimilation to improve global analyses for climate research. Traditionally, NWP centers have used forecast performance as a measure of the quality of the analysis. The notion that a better analysis is prerequisite for a better forecast implicitly assumes that the forecast model is perfect and that forecast errors arise solely from imperfect initial or boundary conditions. In reality, a poor forecast may result from deficiencies in model physics as well as errors in initial and boundary conditions. Initialization procedures can generally yield a better forecast but may not improve the analysis. Conversely, improvements in the analysis do not always lead to significant forecast improvements.

The estimation theory on which modern data assimilation systems are based (e.g., Cohn 1997) provides a

* Current affiliation: Orbital Sciences Corporation, Germantown, Maryland.
+ Additional affiliation: General Sciences Corp., a subsidiary of Science Applications International Corp., Beltsville, Maryland.
# Additional affiliation: Science Systems and Applications Inc., Lanham, Maryland.

Corresponding author address: Dr. Arthur Y. Hou, Code 910.3, NASA Goddard Space Flight Center, Greenbelt, MD 20771.
E-mail: arthur.hou@gsfc.nasa.gov

framework for considering model and observation uncertainties. An optimal data assimilation algorithm provides an estimate of the atmospheric state by taking proper account of these uncertainties. But in the presence of biases in the forecast model, the possibility exists that improving the time-averaged climate signals in an analysis does not necessarily improve, or may even degrade, the short-term forecast. The quality of a climate dataset ultimately rests upon its ability to identify or resolve specific climate issues. While errors in the analysis can affect the forecast accuracy, they might render the analysis altogether inadequate for addressing certain climate problems. Deficiencies of this type cannot be gauged in terms of forecast performance. But if assimilation of a data type improves the ''climate content'' in the analysis but degrades the forecast at the same time, it would imply some internal inconsistency in the assimilation system. One issue we will investigate in this study is whether improving climate signals in an analysis necessarily mean comparable improvements in the 6-h forecast.

The region of the globe where rainfall assimilation may be expected to have the largest impact is the Tropics, where moist convection plays a prominent role and links directly to latent heating, cloud cover, humidity, and the divergent component of the large-scale circulation. The Tropics is also where the analyses by different assimilation systems show significant discrepancies (WCRP 1997). Given the sparse conventional observational network in the Tropics, tropical analysis is understandably sensitive to the first guess, which is, in turn, sensitive to physical parameterization schemes (e.g., Trenberth and Olson 1988) and can suffer from spinup problems (Illari 1987). Previous studies have shown that forecast models have little skill in precipitation forecast in the Tropics (Caplan et al. 1993; Fiorino et al. 1993). While monthly mean precipitation analyses appear to be ''reasonable'' compared with satellite estimates (Janowiak 1992; White et al. 1993), quantitative discrepancies between analyses and observations are still large (see Adler et al. 1996). Misrepresentations in tropical precipitation in the analysis would mean that fields directly linked to rainfall such as moisture, cloud, radiation, vertical motion, and the associated horizontally divergent flow likely have significant errors. Uncertainty in the tropical analysis thus becomes a fundamental issue when applying a multiyear dataset to climate variability studies.

While improving the quality of tropical analyses is crucial to the utility of global analyses in climate applications, the lack of rainfall observations in the Tropics has made it difficult to quantify errors in precipitation and their impact on the analysis. In the past decade the use of satellite-borne microwave instruments has improved the quality and coverage of physically retrieved rainfall estimates. The recent launch of the U.S.–Japan Tropical Rainfall Measuring Mission (TRMM) is expected to further improve observations of tropical rainfall in the coming years. Assimilation of satellite-derived rainfall and related data types offers a way to compensate for model deficiencies and tightens estimates of tropical atmospheric parameters given by different assimilation systems.

Studies have shown that use of satellite-derived rain rate in diabatic or physical initialization can reduce model spinup and improve the short-range forecast, which, in turn, can improve the first guess for the analysis (Krishnamurti et al. 1984, 1991, 1993; Donner 1988; Turpeinen et al. 1990; Puri and Miller 1990; Heckley et al. 1990; Mathur et al. 1992; Kasahara et al. 1994; Manobianco et al. 1994; van Tuyl 1996; Peng and Chang 1996; Treadon 1996, 1997). Despite the positive impact on forecast, this approach has certain drawbacks. Precipitation estimates based on short-term forecasts contain spinup effects, and the model retains little of the improvement beyond 24 h. Moreover, the impact of physical initialization on forecast can be sensitive to the rainfall retrieval algorithm (Krishnamurti et al. 1994) and the methodology does not consider model or observation errors.

Alternatively, rainfall data may be used to directly constrain precipitation in 4D data assimilation. Zupanski and Mesinger (1995) and Tsuyuki (1996a,b, 1997) have shown that 4D-Var rainfall assimilation can improve both forecasts and analyses. Typically a 4D-Var scheme seeks a maximum likelihood estimate assuming a perfect model and a normally distributed observation error, although it is possible to take the model error into account (Derber 1989; Zupanski 1997). The 4D-Var scheme is computationally expensive. Its implementation requires suppression of gravity waves and usually employs a tangent linear model to improve efficiency. The tangent linear approximation may be acceptable for dynamics but might be less valid for rapid nonlinear processes such as moist convection and cloud–solar radiation interaction (Vukicevic and Errico 1993; Errico and Raeder 1999). In some cases it also requires a careful treatment of discontinuities in model physics (D. Zupanski 1993).

In this paper we describe a procedure for assimilating 6-h average surface rainfall and TPW estimates derived from the Special Sensor Microwave/Imager (SSM/I) instruments and examine the impact of these data types on the analysis produced by the Goddard Earth Observing System (GEOS) Data Assimilation System (DAS). A unique feature of the GEOS DAS is that it uses the ''incremental analysis update'' (IAU) procedure of Bloom et al. (1996), which virtually eliminates the spinup problem. The GEOS assimilation is essentially a time-continuous model integration with a gradual insertion of IAU tendencies on prognostic variables updated from observations every 6 h, which is the width of the analysis window. The advantage of this procedure is that it allows fields such as precipitation and evaporation being computed from a continuous model in-

tegration, rather than from short-term forecasts as in other systems.

The general formulation of the procedure we use is based on a 6-h time integration of a column version of the GEOS GCM with full model physics, with the advective terms as ''model forcing'' terms along with the conventional IAU tendencies prescribed from a preliminary 6-h assimilation. We shall refer to this as a procedure in 1+1D, to differentiate it from one involving two spatial dimensions. The control variables are analysis increments of moisture and temperature within the IAU framework. The procedure minimizes the least squares differences between the SSM/I observations and the corresponding values generated by the column model averaged over the 6-h analysis window. The minimization procedure is one-dimensional but the evaluation of the cost function involves a 6-h time integration. Unlike the standard 4D-Var algorithms, which uses the model as a strong constraint, our formulation does not make the ''perfect model'' assumption. Instead, we estimate the model forcing terms as in the continuous variational assimilation (Derber 1989; M. Zupanski 1993). Such a 1+1D assimilation procedure may be viewed as an interactive ''convective retrieval,'' which may be consistently assimilated in the Physical-space Statistical Analysis System (PSAS) framework of the GEOS DAS (Cohn et al. 1998) using the information-content-based algorithms discussed in Joiner and da Silva (1998). The observation and model forcing error covariances may be modeled statistically using observation minus 6-h forecast residuals (Dee and da Silva 1999; Dee et al. 1999).

As a first step in developing the general procedure, in this paper we consider the limiting case of small observation errors relative to model physics errors to obtain a baseline for gauging improvements through error covariance modeling. In this ''perfect observation'' limit, we will use SSM/I rainfall and TPW as strong constraints, as in the physical initialization scheme of Krishnamurti et al. (1984, 1991). Given the positive impact of physical initialization on precipitation forecast, we seek to establish that assimilating these data without knowing their error characteristics can, in fact, improve the analysis. Error covariance information could then be used to optimize the data impact. As in physical initialization, we modify the moisture but not the temperature to match the observed rain rate by performing a minimization with respect to moisture analysis increments of a particular form. This is a reasonable starting point since the uncertainty in the moisture analysis is typically larger than that in temperature. In practice, this simplification reduces a multivariate minimization problem (as in Fillion and Errico 1997) to a univariate, two-parameter minimization for matching the observed precipitation and TPW. In this perfect-observation moisture-adjustment study we focus on two key questions: First, is there useful information in SSM/I rainfall and TPW retrievals without error specifications? Second, are the physical parameterizations in the GEOS DAS good enough to capitalize on this information?

As discussed earlier, an improved estimate of tropical precipitation should improve latent heating, clouds, vertical velocity, and the outgoing longwave radiation (OLR) in the tropical analysis. Among these, OLR observations have by far the best sampling frequency, coverage, and accuracy. Since OLR observations are currently not assimilated in the GEOS DAS, we can use them as verification data to evaluate the impact of rainfall and TPW assimilation on the overall quality of the assimilation. In addition, we will compare results with cloud observations from the International Satellite Cloud Climatology Project (ISCCP) and satellite–model estimates of surface solar radiation. We will also compute brightness temperatures for spectral channels of TIROS Operational Vertical Sounder (TOVS) instruments using temperatures and moisture from the GEOS analyses and compare them with cloud-cleared TOVS measurements to investigate the impact of rainfall and TPW assimilation on the analyses.

Section 2 describes the SSM/I precipitation and TPW datasets. Section 3 describes the 1+1D rainfall and TPW assimilation scheme. Section 4 examines the impact of rainfall and TPW assimilation on time-averaged fields. Section 5 examines the impact on model forecasts. Section 6 discusses comparisons with TOVS radiances. Section 7 investigates the sensitivity of our results to the observed rainfall intensity, and section 8 summarizes our main results.

2. SSM/I precipitation and TPW estimates

The SSM/I surface rain rate used in this study is produced at the National Aeronautics and Space Administration/Goddard Space Flight Center (NASA/GSFC) using the Goddard Profiling (GPROF) Algorithm version 3.3. The GPROF algorithm is a physically based retrieval of vertical hydrometeor profiles that best fits the brightness temperatures in the available passive radiometer channels. The matching uses a library of hydrometeor profiles generated by a numerical cloud model, with each profile associated with a surface precipitation rate. The algorithm retrieves all parameters using the Bayesian method that relies on the estimated expected value, as described in Kummerow et al. (1996) and Olson et al. (1996). The rain rates are obtained from the seven channels of data from the SSM/I instruments aboard the polar-orbiting Defense Meteorological Satellite Program (DMSP) *F10* and *F11* satellites. For applications to the GEOS DAS, the instantaneous SSM/I surface rain rates are horizontally averaged to 2° lat × 2.5° long grid boxes and time averaged over 6 h centered at analysis times (0000, 0600, 1200, 1800 UTC). Although the GPROF algorithm provides global estimates of several parameters, including fractional convective and stratiform rain rates, as well as precipitating and

nonprecipitating liquid and ice, we assimilate only the surface rain rate between 30°S and 30°N in this study.

The instantaneous gridded rain rates have relatively low random error due to sampling, since the pixels completely cover the area within each 2° × 2.5° grid box on a full-view overpass. However, algorithmic error, including viewing geometry effects, can be important. Experience shows that individual GPROF pixel rain-rate estimates have a random error of about 50% (Kummerow et al. 1996) at moderate rain rates in the Tropics. Following the analysis of Bell et al. (1990), averaging these estimates from a single full overpass over a 2° × 2.5° grid box reduces the random error to about 10%. Additional uncertainty is introduced because each grid box is observed only once or twice (if at all) in a 6-h accumulation period. This sparse sampling results from the limited swaths typical of polar-orbit instruments (cf. TRMM 1996). In an unpublished work Kummerow sampled Tropical Ocean Global Atmosphere Coupled Ocean–Atmosphere Response Experiment radar rain rates at SSM/I observing times and estimated random errors due to sampling in time to be 30% for 6-h accumulations on a 2.5° × 2.5° grid. One complication in this discussion is that the relative (percent) random error varies roughly as the inverse square root of the rain rate, so that relative random errors are significantly worse in light rain areas, but somewhat better in heavy rain areas (Huffman 1997).

The global bias field is not yet established for GPROF estimates, since most regions lack the necessary validation data and no statistical model has been developed to estimate bias from other parameters. On the monthly timescale, the two-satellite GPROF estimates showed a correlation of 0.69 and a bias of 19% against a thin scattering of gauge-based validation grid boxes around the globe (mostly on land) for all of 1992 (Adler et al. 1996). In the same study comparisons of two-satellite GPROF estimates and tropical Pacific atoll rain gauges yielded a correlation of 0.72 and a bias of 23%. Synthetic retrieval studies show that the bias in GPROF estimates over land is roughly twice that over ocean (W. S. Olson 1998, personal communication). Studies that validate satellite estimates with radar frequently find larger biases, but the comparability of satellite and radar results remains open to debate (Smith et al. 1998).

For TPW estimates, we use the physically retrieved SSM/I-2 product over oceans derived from the SSM/I instruments aboard the *F10* and *F11* DMSP satellites (Wentz 1994). The SSM/I-2 water vapor is improved over the SSM/I-1 retrieval with a better specification for the effective air temperature. The SSM/I-2 algorithm is fine-tuned to 35 000 radiosonde water vapor contents. The physical parameters in the model such as water vapor absorption etc. are adjusted to minimize the difference between SSM/I retrievals and the in situ measurements. For a spatial resolution of 50 km over ocean scenes free of rain, the rms accuracy for the retrieved columnar water vapor is estimated to be about 0.1 cm. The analysis by Wentz (1997) using data from 1987–90 suggests a systematic error that is less than the rms error—around 0.06 cm. As with rain rates, we assimilate only TPW estimates between 30°S and 30°N in this study.

3. Methodology

a. The GEOS Data Assimilation System

The data assimilation system used in this study is an intermediate system between the GEOS-1 DAS (Pfaendtner et al. 1995) used to produce the first NASA reanalysis and the GEOS-2 DAS with the PSAS (Cohn et al. 1998). The system employs the second generation of the GEOS GCM (GEOS-2 GCM, version 5.9) and version 1.5 of the optimal interpolation (OI) analysis scheme (DAO 1996). The prognostic variables are potential temperature, specific humidity, surface pressure, and winds in the zonal and meridional directions, computed at the resolution of 2° latitude, 2.5° longitude, and 46 σ levels from the surface to 0.4 hPa, using a Matsuno time step of 2.5 min. The moist physics are parameterized using the relaxed Arakawa–Schubert scheme for penetrative convection (Moorthi and Suarez 1992) coupled to a Kessler-type of reevaporation of falling rain and large-scale precipitation due to supersaturation (see DAO 1996 for details). The physics tendencies are updated every 10 min for moist processes, 30 min for turbulence, and 3 h for radiation.

The OI analysis scheme and statistics are described in Pfaendtner et al. (1995). The upper-air height and wind analyses and the sea level surface wind analyses are performed every 6 h using multivariate statistical interpolation algorithms on 18 pressure levels. The moisture analysis is done using a univariate statistical algorithm between 300 hPa and the surface. The conventional observations are from rawinsondes, dropsondes, rocketsondes, aircraft winds, cloud-tracked winds, and thicknesses from historical TOVS soundings from the National Environmental Satellite, Data and Information Service.

The GEOS DAS employs no explicit initialization but relies on the IAU procedure of Bloom et al. (1996) to reduce any imbalance that might occur due to data ingestion. The procedure first computes for each prognostic variable a total analysis increment using 6-h averaged observations centered at the analysis times. These total analysis increments are then divided by the number of time steps over the 6 h to produce IAU tendencies to be added at each time step as additional forcing terms in the prognostic equations during the assimilation. An advantage of this procedure is that there is no obvious spinup in the precipitation and evaporation fields in what is essentially a continuous model integration with a gradual insertion of data constraints (Schubert et al. 1993; Bloom et al 1996).

b. The general 1+1D estimation procedure for assimilating nonstate variables

In global GCMs the convective processes are typically modeled in a vertical column of the atmosphere. In radiative transfer models the reduced dimensionality to a single column allows the development of efficient 1D retrieval algorithms of temperature and moisture information from radiance measurements. Similarly, one could use ''convective observations'' such as surface rain rate to obtain information about the thermodynamic structure of the atmosphere. But surface precipitation observations alone do not contain sufficient information for determining vertical profiles of temperature and moisture, as it contains exactly one piece of information. The profiles ''retrieved'' from these data types must therefore be constrained and consequently strongly influenced by the first guess. Such retrievals can be modified to extract the actual information content from the radiance measurement for consistent assimilation, as proposed by Joiner and da Silva (1998). But in this study we will eschew such refinement in the initial implementation of the general procedure. Instead, we reduce the dimensionality of the problem by adopting a particular form of analysis increments with two free parameters to accommodate the two pieces of information provided by precipitation and TPW observations (cf. section 3c).

Assimilating a given data type stipulates that a relationship exists between the model variables and the quantity being assimilated. Convective parameterizations in global GCMs are generally not cloud resolving, with clouds and precipitation represented as ensemble means in a grid box over a convective timescale of a few hours. It is therefore not physically consistent to assimilate instantaneous rain rate in a non-cloud-resolving model. In this study we will assimilate the 6-h averaged SSM/I rain rate and TPW over a grid box into the GEOS DAS. We describe in this section a general procedure for estimating the vertical thermodynamic structure of the atmosphere using convective observations that involves a time integration of a simplified column version of the GCM. To distinguish this from a procedure in two spatial dimensions, we shall refer to this as an estimation problem in 1 + 1 dimensions. Let $\mathbf{w} = [\theta\ q]^{\mathrm{T}}$ be the thermodynamic state vector for an atmospheric column, consisting of profiles of potential temperature, θ, and specific humidity, q. The prognostic equation for $\mathbf{w}$ in the GEOS DAS is

$$\frac{\partial \mathbf{w}}{\partial t} = \mathbf{F}_{\mathrm{adv}} + \mathbf{F}_{\mathrm{moist}} + \mathbf{F}_{\mathrm{rad}} + \mathbf{F}_{\mathrm{turb}} + \frac{\Delta \mathbf{w}}{\tau}, \qquad (1)$$

where $\mathbf{F}_{\mathrm{adv}}$, $\mathbf{F}_{\mathrm{moist}}$, $\mathbf{F}_{\mathrm{rad}}$, and $\mathbf{F}_{\mathrm{turb}}$ are the tendency terms due to advection, moist processes, radiation, and turbulence, respectively. The last term, $\Delta\mathbf{w}/\tau$, is an IAU forcing consisting of the analysis increment, $\Delta\mathbf{w}$ (the difference between the analysis and the first guess updated every assimilation cycle), normalized by the width of the analysis window, τ (Bloom et al. 1996). If the advective tendency, $\mathbf{F}_{\mathrm{adv}}$, can be prescribed, then (1) becomes a 1D prognostic equation of processes in an atmospheric column. This one-dimensional prognostic equation will be the basis for our 1+1D assimilation scheme.

To assimilate a specific type of observations available from $t = -\tau/2$ to $t = +\tau/2$ (where τ is typically 6 h) in an assimilation cycle centered at $t = 0$, we seek the ''IAU parameter estimate,'' $\Delta\mathbf{w}$, that yields assimilation fields that best match observations based on the relative uncertainties of the observations and a prior parameter estimate, $\Delta\mathbf{w}^{-} = 0$. Formally, we minimize the following functional, $J(\Delta\mathbf{w})$:

$$J(\Delta\mathbf{w}) = \Delta\mathbf{w}^{\mathrm{T}}\mathbf{Q}^{-1}\Delta\mathbf{w} + \sum_{k} [\mathbf{w}_k^o - h_k(\Delta\mathbf{w})]^{\mathrm{T}}\mathbf{R}_k^{-1}[\mathbf{w}_k^o - h_k(\Delta\mathbf{w})], \qquad (2)$$

where $\mathbf{Q}$ is the error covariance matrix of the prior estimate $\Delta\mathbf{w}^{-}$, $\mathbf{w}_k^o$ is the instantaneous or time-mean observation vector at $t = t_k$, and $h_k(\Delta\mathbf{w})$ is the observation operator that provides a model estimate of the observable at $t = t_k$ for a given value of $\Delta\mathbf{w}$. For applications to time-averaged data, we can omit the subscript k and take $h(\Delta\mathbf{w})$ to be the time-averaged observable. For precipitation assimilation in the GEOS DAS, we take $h(\Delta\mathbf{w})$ to be the natural log of the 6-h, gridbox-averaged surface precipitation obtained by integrating (1), for a given $\Delta\mathbf{w}$, from $t = -\tau/2$ to $t = +\tau/2$ with $\mathbf{F}_{\mathrm{adv}}$, $\mathbf{F}_{\mathrm{rad}}$, and $\mathbf{F}_{\mathrm{turb}}$ prescribed from a 3D first-guess assimilation without precipitation data (see sections 3c and 3d). During this assimilation cycle, surface precipitation is obtained by computing $\mathbf{F}_{\mathrm{moist}}$ explicitly using the same moist physics as in the GEOS GCM. The ''observation'' error covariance $\mathbf{R}$ in (2) includes both errors in the observations $\mathbf{w}^o$ as well as errors in the forward model, $h(\Delta\mathbf{w})$. The implicit assumption here is that observations and IAU parameter estimates are unbiased, with normally distributed random errors that are uncorrelated in time. The IAU forcing $\Delta\mathbf{w}/\tau$ may be interpreted as a correction that compensates for the net model deficiency, acting as a synoptically varying bias correction term.

The 1+1D scheme described above is closely related to the 4D-Var formulation. The estimation problem defined by (2) may be generalized to 4D by replacing the column model (1) with the full GEOS GCM and extending the control variable $\Delta\mathbf{w}$ to include increments of all state variables in three dimensions. The resulting 4D formulation differs from the standard 4D-Var algorithm in its choice of control variable: instead of estimating the initial condition at the beginning of the assimilation cycle, we estimate the IAU forcing to be applied throughout the assimilation cycle and, in doing so, impose the forecast model as a *weak constraint* in a manner similar to the variational continuous assimilation technique proposed by Derber (1989), although Derber did not explicitly include parameter and obser-

vation error covariances. M. Zupanski (1993) extended Derber's scheme in the 4D-Var context to simultaneously estimate a constant, IAU-like forcing term and the initial condition at the beginning of the assimilation cycle, but found the impact of this extra degree of freedom was modest, despite the increased computational expense. Zupanski (1997) proposed for operational 4D-Var systems a more general weak constraint that allows the estimated forcing term to vary in time. Although this approach may also be used in our 1+1D context, we have not adopted it since applying a constant forcing over a 6-h interval is more consistent with the IAU formulation used in the GEOS DAS and is easier to implement.

c. A 1+1D moisture-adjustment procedure in the perfect observation limit

The minimization of the functional (2) requires the specification of the error covariances $\mathbf{Q}$ and $\mathbf{R}$, which may, in principle, be modeled statistically from innovation time series (Dee and da Silva 1999; Dee et al. 1999). As a first step in developing a statistical approach to rainfall and TPW assimilation, here we consider the limiting case of small observation errors relative to errors in the IAU parameter estimate. Such a perfect observation study provides a baseline for evaluating error covariance models for optimal use of these data types. The perfect observation assumption was also used to good advantage in physical initialization studies (Krishnamurti et al. 1991, 1993, 1994). As in physical initialization, we will adjust only the moisture profile. Specifically, we make the following assumptions.

1) We assume that uncertainties in the moisture variable are much larger than those in the temperature field and that errors in these fields are uncorrelated. More precisely, if we write $\mathbf{Q}$ as

$$\mathbf{Q} = \begin{bmatrix} \mathbf{Q}_{\theta,\theta} & \mathbf{Q}_{\theta,q} \\ \mathbf{Q}_{q,\theta} & \mathbf{Q}_{q,q} \end{bmatrix}, \tag{3}$$

we assume that $\|\mathbf{Q}_{\theta\theta}\| \gg \|\mathbf{Q}_{qq}\|$ and $\|\mathbf{Q}_{q\theta}\| = \|\mathbf{Q}_{\theta q}\| = 0$, which leads to $\Delta\mathbf{w} = [\Delta\theta \ \Delta q] = [0 \ \Delta q]$. Under these assumption, (2) reduces to

$$J(\Delta q) = \Delta q^{\mathrm{T}}\mathbf{Q}_{qq}^{-1}\Delta q + [\mathbf{w}^o - h(\Delta q)]^{\mathrm{T}}\mathbf{R}^{-1}[\mathbf{w}^o - h(\Delta q)]. \tag{4a}$$

2) To further reduce the dimensionality of the problem, we prescribe the vertical structure of the moisture increment, Δq. This is equivalent to modeling $\mathbf{Q}_{qq}$ as a reduced rank matrix with the prescribed profile defining the subspace where the parameter estimate uncertainty lies.
3) Finally, we restrict consideration to the perfect observation limit, $\|\mathbf{Q}_{qq}\| \gg \|\mathbf{R}\|$, which allows us to neglect the first term on the rhs of (4a).

With the above assumptions, the 1+1D procedure was implemented in the GEOS DAS as follows: At each grid box where the difference between the observed 6-h rain rate, P^o, and the model-generated rain rate, P^f, exceeds 1 mm day^{-1}, we minimize the functional

$$J(\Delta q) = \{\ln(P^o + \epsilon) - \ln[P^f(\Delta q) + \epsilon]\}^2, \tag{4b}$$

where Δq is the moisture increment over the 6-h analysis window and ϵ is a small constant used to prevent logarithmic singularity at zero rain rate (taken to be 0.01 mm day^{-1}). The quantities, $\mathbf{w}^o = \ln(P^o + \epsilon)$ and $h(\Delta q) = \ln[P^f(\Delta q) + \epsilon]$, are assumed to be unbiased and normally distributed; (4b) is a generalized log-normal distribution that remains valid for zero values of precipitation. Here, P^f is obtained by integrating (1) for $\mathbf{w} = [\theta \ q]$ from $t = -\tau/2$ to $t = +\tau/2$, with $\mathbf{F}_{\mathrm{adv}}$, $\mathbf{F}_{\mathrm{rad}}$, and $\mathbf{F}_{\mathrm{turb}}$ prescribed from a first-guess assimilation with all observations except precipitation (see section 3d for details); P^f is diagnosed from the moist physics module used in computing $\mathbf{F}_{\mathrm{moist}}(\theta, q)$.

In the absence of a "background" term, the minimization of the functional (4b) is ill-posed since a single piece of information in precipitation discrepancy is not sufficient to determine the variation of Δq with height. Consistent with assumption (2) and similar to the method used by Treadon (1996) and van Tuyl (1996), we model the moisture increment in terms of a change in relative humidity, Δr:

$$\Delta q = q_s(T)\Delta r, \tag{5}$$

where $q_s(T)$ is the saturation specific humidity and

$$\Delta r = \begin{cases} \alpha \ln(p) + \beta & \text{for } p > p^* \\ 0 & \text{otherwise} \end{cases} \tag{6}$$

with p^* set to 100 hPa. Equation (6) contains two parameters to accommodate the two pieces of information provided by the precipitation and TPW retrievals, with α modifying the slope of Δr to match the observed rain rate and β matching the observed TPW. At locations with a valid SSM/I TPW observation, the vertically integrated column moisture increment can be determined from SSM/I retrieval of TPW, $\overline{q}^o$, and the model first guess, $\overline{q}^f$:

$$\Delta\overline{q} \equiv \int_0^{p_s} \Delta q \, \frac{dp}{g} = \overline{q}^o - \overline{q}^f. \tag{7}$$

If SSM/I TPW data are not used, $\Delta\overline{q}$ is set to zero, so that the moisture increment due to precipitation data introduces no net moisture source in a vertical column. (This does not mean that $\overline{q}$ is conserved during the assimilation cycle, see section 3e.) Combining (5)–(7), we obtain Δq in terms of a single parameter, α:

$$\Delta q(\alpha) = q_s(T)\left\{\left[\ln(p) - \frac{\overline{q_s \ln(p)}}{\overline{q_s}}\right]\alpha + \frac{\Delta\overline{q}}{\overline{q_s}}\right\}, \quad \text{for } p > p^*. \tag{8}$$

Substituting (8) into (4b) reduces the problem to a 1D

minimization of $J[\Delta q(\alpha)]$ w.r.t. α for given values of P^o and $\overline{q}^o$.

As mentioned earlier, the 1+1D moisture-adjustment, perfect observation scheme shares similar assumptions as those used in physical initialization. But as a data assimilation scheme, the impact of physical initialization is fundamentally different from that of the 1+1D scheme on the analysis. Physical initialization is used to improve the first guess used at a given analysis time by nudging the precipitation forecast from a previous analysis (Treadon 1996), whereas the 1+1D scheme implemented in the IAU framework constrains the assimilation system to produce the 6-h average rain rate and TPW best matching the observations within a given analysis window.

d. Implementation in the GEOS DAS

As noted in section 3a, the moisture analysis in the GEOS DAS is univariate, with specific humidity analysis increments determined independent of the temperature field. Currently only radiosonde observations are used in the moisture analysis, with analysis increments concentrated over land and around tropical islands. The procedure for computing the moisture analysis increment, Δq, due to precipitation and TPW is as follows.

1) We first compute the IAU increments due to all conventional data types (not including rainfall or TPW data) as in a standard operational 6-h GEOS DAS assimilation.
2) At grid boxes with SSM/I TPW retrievals, we compute a TPW-induced moisture IAU increment by scaling the first-guess moisture profile to match the observed TPW using a procedure similar to that described in Ledvina and Pfaendtner (1995) but with only one iteration. We then add these TPW-induced moisture IAU increments to moisture analysis increments due to other data types used in the operational GEOS DAS (which currently consist of only rawinsonde observations) and use a Cressman weighted-mean method with a 500-km radius to smooth the combined increments over the neighboring grid boxes.
3) We then perform a preliminary 3-h global assimilation without rainfall data using all conventional and TPW (if available) data to produce 3-h averaged $\mathbf{F}_{\text{adv}}$, $\mathbf{F}_{\text{rad}}$, and $\mathbf{F}_{\text{turb}}$ tendencies.
4) At every grid box with precipitation observation, we use these 3-h averaged $\mathbf{F}_{\text{adv}}$, $\mathbf{F}_{\text{rad}}$, and $\mathbf{F}_{\text{turb}}$ to integrate (1) forward in time to obtain the 6-h mean precipitation, P^f, for a given value of α to evaluate the cost function, $J(\alpha)$. The reason for using 3-h averaged $\mathbf{F}_{\text{adv}}$, $\mathbf{F}_{\text{rad}}$, and $\mathbf{F}_{\text{turb}}$ is purely economical. Diagnostics show that these fields are slowly varying. The cost function calculated using the 3-h mean forcing is within 10% of that computed using the 6-h time series of these forcing terms.
5) The cost function $J(\alpha)$ is then minimized w.r.t. α using an iterative procedure starting from $\alpha = 0$ and searching over the interval between -2 and 2 (see below). The vertical profile of Δq is obtained by evaluating (8) at the minimization point for $\alpha = \alpha_{\min}$.
6) Once we have obtained the Δq increments due to precipitation and/or TPW for all grid boxes with SSM/I observations, we combine them with moisture analysis increments due to conventional data, as described in 2 above. The resulting 3D moisture analysis increments are then divided by 6 h to produce the total moisture IAU tendency for the final assimilation. The successive correction procedure also has the advantage of adding a degree of spatial coherence to the Δq increments due to TPW and precipitation data.

The minimization algorithm based on a golden section search and successive parabolic interpolation (Press et al. 1992) is quite robust, with the solution obtained typically in less than 14 iterations (see Fig. 1c). The search interval is chosen experimentally. Analysis showed that with $-2 \leq \alpha \leq 2$, $J(\alpha)$ attains a unique global minimum at roughly 85% of all minimization locations in the Tropics. In the remaining cases the solution still provides a better match with the observation, though not a true minimum. Expending the search interval increases the cases of true minimum but can lead to excessively large moisture changes in the atmospheric interior (see section 6). We analyzed the variation of the cost function with α as a parameter for a large selection of tropical locations and found that on rare occasions $J(\alpha)$ may have a maximum within $-2 \leq \alpha \leq 2$, so that the solution is not unique. Identifying such cases would require an elaborate testing procedure evaluating the cost function in α space at each minimization location. Since each $J(\alpha)$ computation requires a 6-h assimilation, implementing this operationally would be prohibitively expensive. Given their rare occurrences, we did not test to remove such cases in the present study.

The degree to which we succeed in matching the 6-h rain rate in the final assimilation with the observed rain rate depends on how rapidly $\mathbf{F}_{\text{adv}}$, $\mathbf{F}_{\text{rad}}$, and $\mathbf{F}_{\text{turb}}$ respond to changes in convection. We found that the net tendency of the time-averaged $\mathbf{F}_{\text{adv}}$, $\mathbf{F}_{\text{rad}}$, and $\mathbf{F}_{\text{turb}}$ differs by about 20% between two 6-h assimilations from the same initial condition with and without SSM/I rain rates. This explains why prescribing the time-average $\mathbf{F}_{\text{adv}}$, $\mathbf{F}_{\text{rad}}$, and $\mathbf{F}_{\text{turb}}$ in (1) with values taken form an assimilation without rainfall data can provide a good estimate of P^f for matching P^o in this 1+1D assimilation procedure.

e. Impact on temperature and moisture at the minimization location

The solution to (4b), $\Delta q(\alpha_{\min})$, divided by 6 h, yields moisture IAU tendencies due to precipitation and TPW observations. The quantity $\Delta q(\alpha_{\min})$ is therefore the 6-h

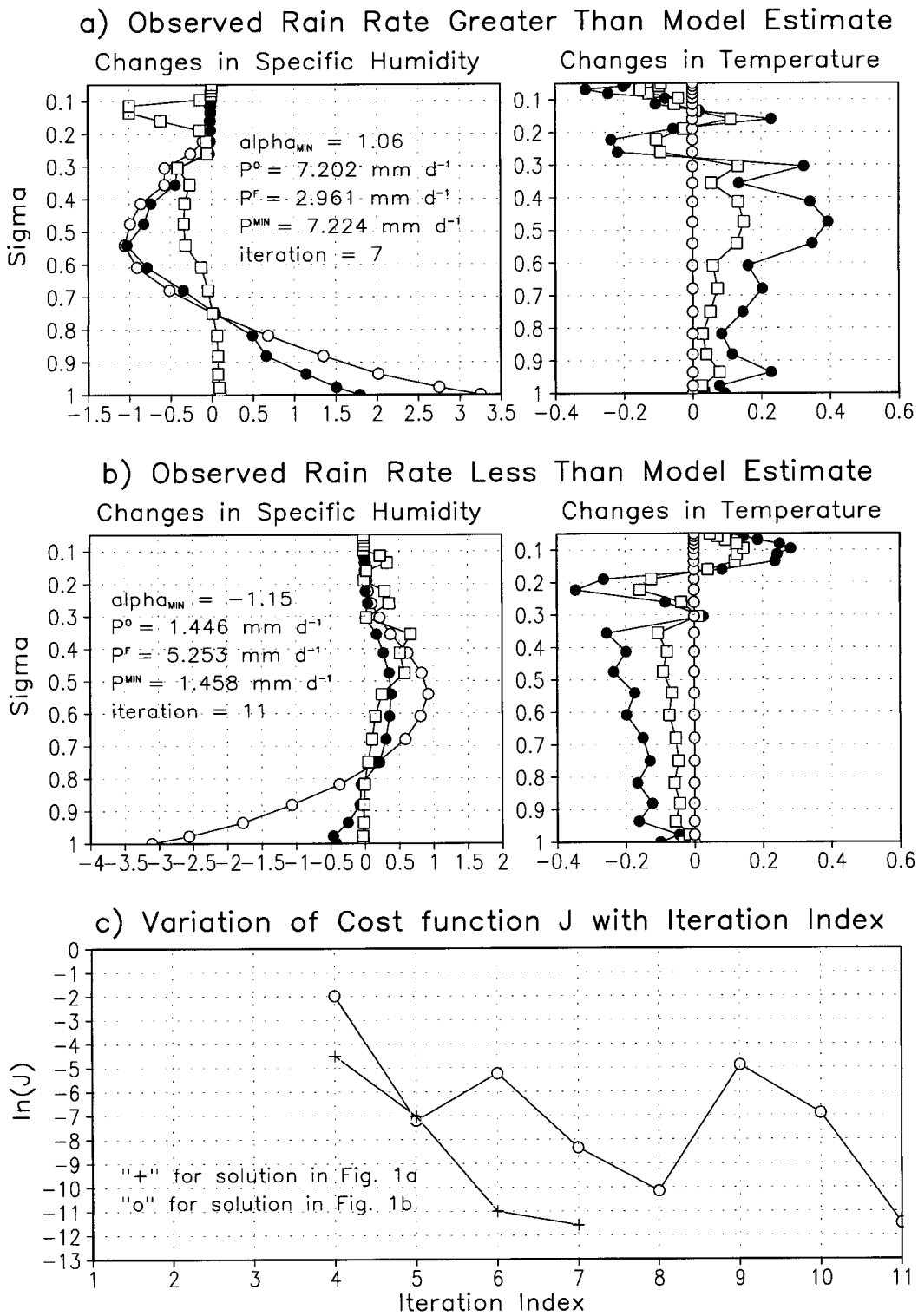

FIG. 1. Temperature and humidity changes (rainfall and TPW assimilation minus control) at two minimization locations. (a) Enhanced precipitation at 6°S, 57.5°E. Left panel shows that changes in specific humidity (g kg^{-1}) at the analysis time (solid circle) are generally smaller the 3-h accumulated rainfall-induced moisture IAU forcing (open circle). The open squares indicate the *fractional* changes. The legend shows the observed rain rate, P^o; the initial guess with $\alpha = 0$, P^F; and the minimization solution, P^{min}. Right panel shows changes in temperature (K) (solid circle) and the corresponding *percentage* changes (open square). The prescribed IAU forcing on temperature due to rainfall/TPW is identically zero by design (open circle). (b) Same as (a) but for reduced precipitation at 10°S, 75°E. (c) Variation of the cost function, *J*, as a function of the iteration index for the solution shown in (a) (open circle) and that in (b) (solid circle).

accumulated IAU forcing prescribed in the moisture equation, which does not equal the net moisture change over the assimilation cycle due to the action of moist physics.

Figure 1 shows the impact of the assimilation procedure on the local moisture and temperature profiles at two grid boxes: one for P^o greater than P^f (Fig. 1a) and one for P^o less than P^f (Fig. 1b). Each case consists of two parallel assimilations with and without SSM/I observations starting from the same initial condition. Since no conventional moisture observations are available at either of these locations, the net change of moisture at the analysis time (at the midpoint of the 6-h window) is the sum of the change due to moist physics and that due to the prescribed rainfall-induced IAU forcing in 3 h, that is, $\frac{1}{2}\Delta q(\alpha_{\min})$. The left panels are comparisons of the actual change in moisture at the analysis time with the 3-h accumulated IAU forcing. The fractional changes in specific humidity (open squares) are small except at the upper levels. The figure legend displays the solution to (4b) with $P^{\min}$ as the 6-h average rain rate given by the minimization procedure. In these examples, $P^{\min}$ is within 1% of the observed rain rate, P^o. Since the moisture adjustment, $\Delta\alpha$, is in the form of a vertical redistribution, enhanced surface precipitation typically leads to drying in the upper troposphere, while reduced precipitation leads to moistening aloft. The impact of rainfall assimilation on the upper-level moisture is further examined in section 6. The right panels of Figs. 1a and 1b show that the minimization has only a minor impact on the temperature—typically less than 0.5 K, or 0.2% throughout the troposphere. Figure 1c is a plot of the functional, J, against the iteration index at these two minimization points.

4. Impact on time-averaged fields

To study the impact of assimilating SSM/-based rainfall and TPW retrievals between 30°S and 30°N on the GEOS analysis, we performed four parallel 1-month assimilations for December 1992. The control is the standard GEOS assimilation described in section 3a, using only conventional observations. In three more cases we assimilate—in addition to conventional observations—either SSM/I rainfall (case A), or SSM/I rainfall and SSM/I TPW (case B), or SSM/I TPW (case C).

a. Surface precipitation

An example of the extent to which rainfall assimilation can match the precipitation from the assimilation with observations in one assimilation cycle is shown in Fig. 2, which compares the 6-h average precipitation with SSM/I GPROF rain rates derived from *F10* and *F11* satellites at 0600 UTC on 1 December 1992. Comparing Fig. 2b with Fig. 2c shows that rainfall assimilation effectively brings the GEOS precipitation closer to the SSM/I data. Rainfall assimilation increases the spatial anomaly correlation from 0.32 to 0.74, and reduces the tropical mean bias by roughly a factor of 2 and the error std dev by 32%. In general, assimilating SSM/I rain rates with or without TPW data significantly improves the anomaly correlation and reduces the error std dev. The tropical-mean biases are typically less than 0.5 mm day^{-1}, within uncertainties of the 6-h SSM/I estimate.

Figure 3a displays the combined *F10* and *F11* SSM/I GPROF rain rate for December, 1992. Fig. 3b shows the difference between the SSM/I rain rate and that from the GEOS control sampled at SSM/I observation locations. Figures 3c and 3d are the corresponding differences for case A (with SSM/I rainfall) and case B (with SSM/I rainfall and TPW), respectively. The spatial error statistics are given in Table 1. Overall, assimilating tropical SSM/I rain rates with or without TPW enhances the spatial correlation of the monthly mean precipitation with observations from 0.53 to over 0.85 and reduces the error std dev by 40%. These reductions are statistically significant with F-test probabilities of less than 1%. The tropical-mean spatial biases are small residuals of positive and negative time-mean biases. The apparent increase in the tropical-mean bias in Fig. 3c reflects that the rainfall assimilation scheme is more effective in reducing the precipitation intensity than enhancing it in matching the GEOS DAS with the SSM/I rain rates. This asymmetry leads to a seemingly larger tropical-averaged monthly mean bias, although the positive and negative time-mean biases in the Tropics are significantly smaller in Fig. 3c than their counterparts in Fig. 3b. The addition of TPW data further increases this asymmetry. The predominantly negative biases in cases A and B are evident in Figs. 3c and 3d, indicating that in certain situations the convective parameterization used in the GEOS DAS cannot match the intense GPROF rain rates within the prescribed adjustment limits. However, a tropical-mean bias of 0.5 mm day^{-1} is comparable to the uncertainty in the monthly mean SSM/I retrieval (cf. section 2), although it is possible that improvements of the convective physics in the GEOS DAS may lead to a better result. Table 1 also shows that assimilating tropical SSM/I TPW alone (case C) does not improve the precipitation, even though it significantly improves the moisture analysis, as shown in the next section.

b. Total precipitable water

Figure 4a shows Wentz's SSM/I TPW retrieval over oceans for December 1992. The difference between the SSM/I TPW and the TPW from the control sampled at SSM/I observation locations is shown in Fig. 4b. Figures 4c and 4d are the corresponding differences for case C (with SSM/I TPW only) and case B (with SSM/I rainfall and TPW), respectively. Table 2

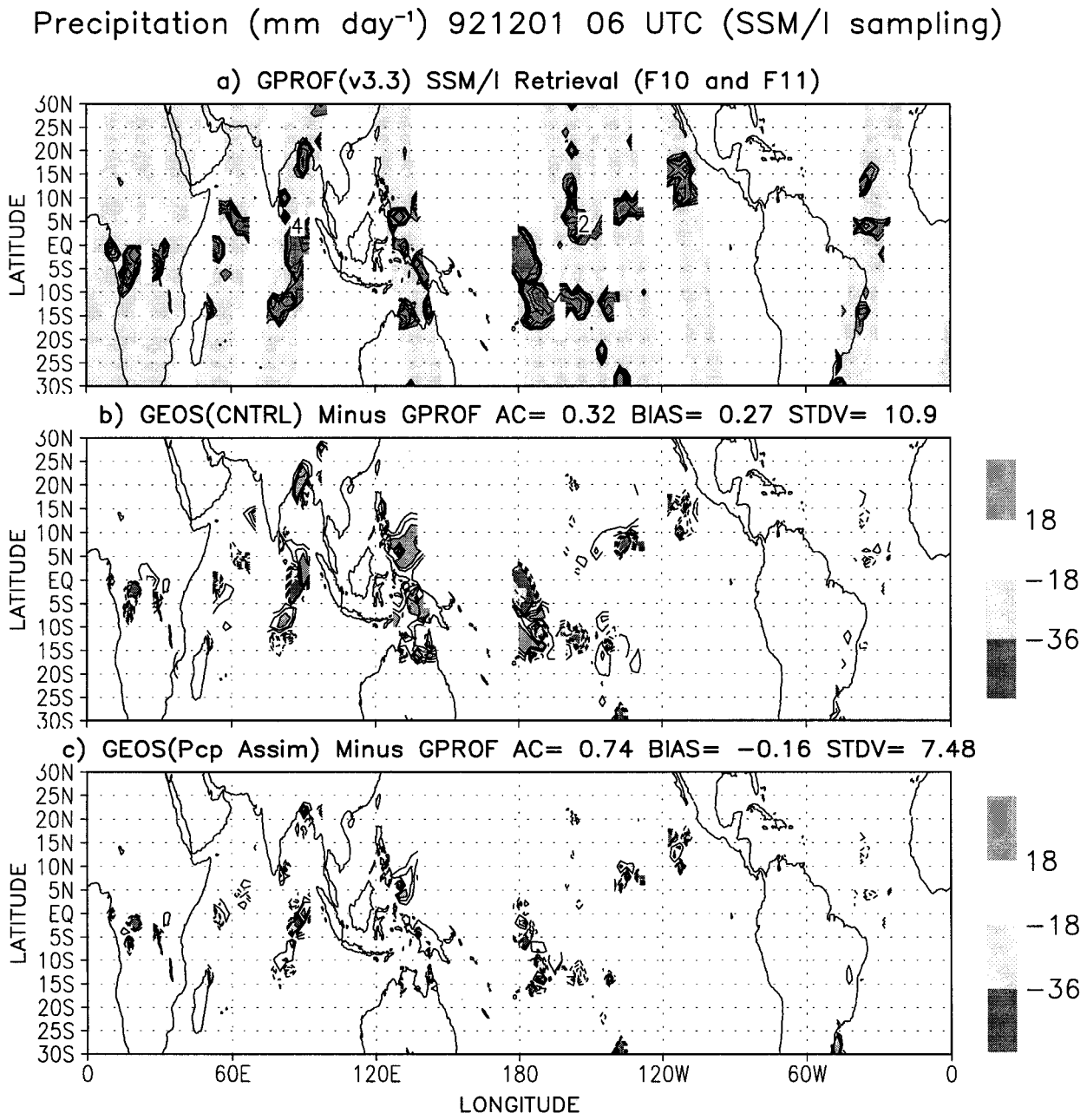

FIG. 2. (a) The 6-h average SSM/I GPROF rain rates based on DMSP satellites *F10* and *F11* at 0600 UTC on 1 Dec 1992. The satellite observation tracks are shaded, with the light shade indicating no precipitation. The dark shade shows rain rates above 2 mm day^{-1}, with contours at 2, 4, 6, 8, 16, and 32 mm day^{-1}. (b) Difference between SSM/I rainfall estimate and precipitation from the control sampled at SSM/I observation locations. The contour interval is 3 mm day^{-1}. Also shown are the computed spatial anomaly correlation (AC), bias, and error std dev. (c) Same as (b) but for case A.

shows that assimilation of tropical SSM/I TPW significantly reduces an existing tropical dry bias in the control and cuts the error std dev by 50%. Using SSM/I rainfall data in conjunction with TPW further reduces the bias and error std dev. But assimilating SSM/I rainfall without TPW (case A) does not improve the TPW analysis.

c. Impact on the large-scale circulation and atmospheric radiation

The chief motivation for assimilating tropical precipitation observation is to improve the latent heating in the assimilation, which, given its dominant role in the Tropics, would, in turn, improve other assimilation

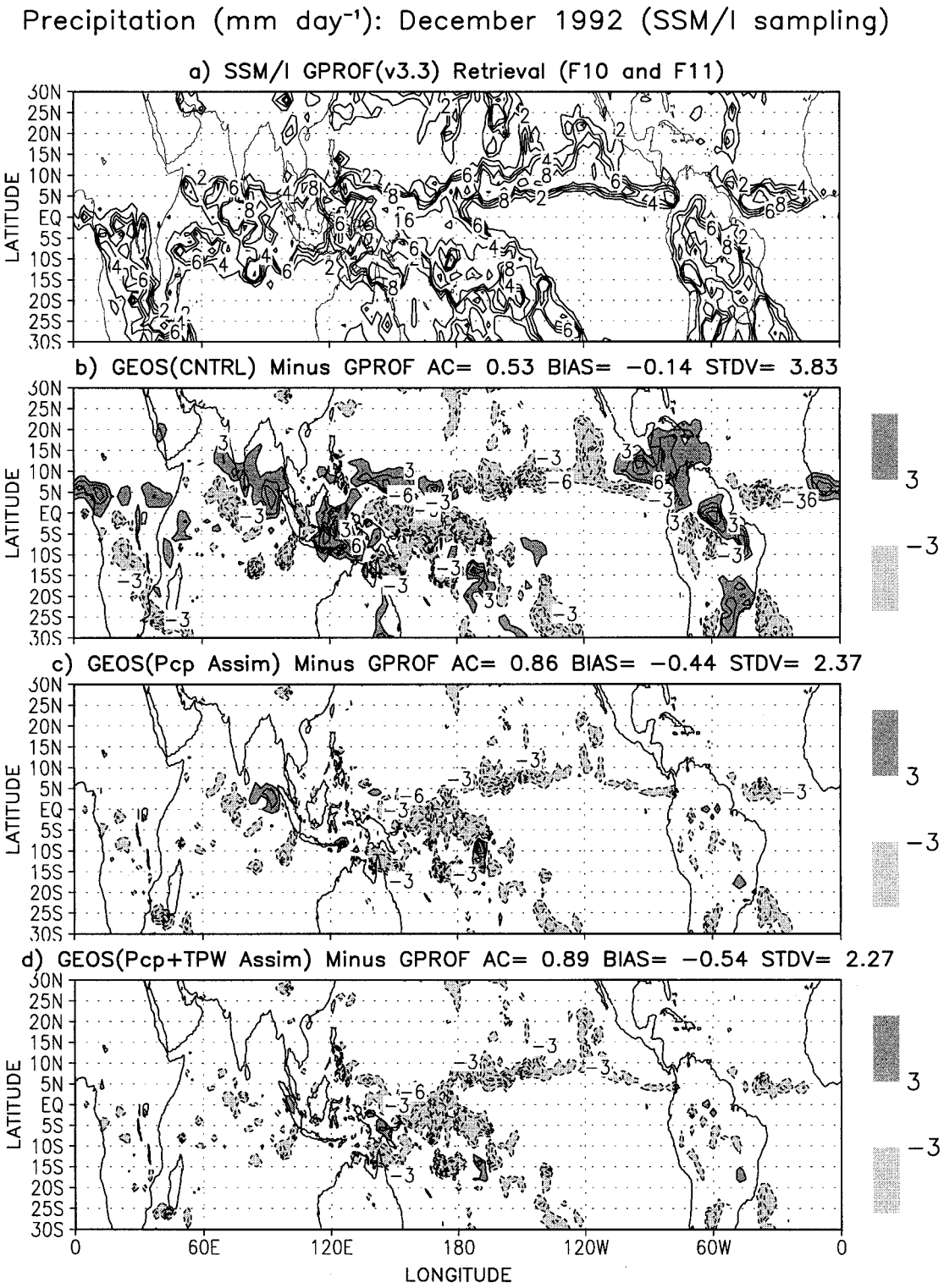

FIG. 3. (a) Time-mean SSM/I GPROF precipitation for Dec 1992. The contours are 2, 4, 6, 8, 16, and 32 mm day^{-1}. (b) Difference between SSM/I rainfall estimate and precipitation from the control sampled at SSM/I observation locations. The contour interval is 3 mm day^{-1}. (c) Same as (b) but for case A. (d) Same as (b) but for case B.

TABLE 1. Spatial statistics of December-mean precipitation minus SSM/I GPROF retrieval 20°S–20°N and 30°S–30°N (in parentheses).

	Anomaly corr	Bias (mm day^{-1})	Error std dev (mm day^{-1})	Std dev change
Control	0.51 (0.53)	−0.08 (−0.14)	4.33 (3.83)	— —
Case A (Pcp)	0.87 (0.86)	−0.56 (−0.44)	2.60 (2.37)	−40.0% (−38.1%)
Case B (Pcp + TPW)	0.89 (0.89)	−0.65 (−0.54)	2.51 (2.27)	−42.1% (−40.7%)
Case C (TPW)	0.59 (0.59)	1.06 (0.71)	4.38 (3.92)	+1.2% (+2.5%)

fields through model physics and dynamics. Figure 5 shows that the improved precipitation in case B directly affects the omega velocity at 500 hPa and the OLR at the top of the atmosphere. The spatial anomaly correlation between the monthly mean precipitation and the 500-hPa omega velocity is −0.80, and that between precipitation and OLR is −0.66. The anomaly correlation between precipitation and the cloudy-sky OLR is even higher, about −0.71 (see Fig. 7a). We obtained similar results for case A without TPW observations. Since the horizontally divergent flow is proportional to the vertical gradient of the vertical velocity, the changes shown in Fig. 5b should indicate an improved divergent component in the large-scale circulation, but this is difficult to confirm due to the paucity of wind data in the Tropics. We can, however, verify whether the OLR in the assimilation is improved through comparisons with satellite observations of OLR, which may be used for validation since they were not assimilated in the GEOS DAS.

d. Comparison with NOAA outgoing longwave radiation

The OLR data we used are estimates derived from the Advanced Very High Resolution Radiometer (AVHRR) instruments on National Oceanic and Atmospheric Administration board polar-orbiting satellites (*NOAA-11* and *-12*). The absolute accuracies of these instruments are difficult to ascertain. Gruber et al. (1994) have shown that the monthly global bias between the narrowband AVHRR channels from the *NOAA-9* and the broadband Earth Radiation Budget Experiment (ERBE) is around 1–2 W m^{-2} in daytime and 4–7 W m^{-2} in nighttime, with rms differences in the 12–15 W m^{-2} range. Our own analysis shows that the NOAA OLR has a low bias up to 10–15 W m^{-2} relative to ERBE data for OLR values greater than 240 W m^{-2}. The AVHRR instruments on *NOAA-11* and *-12* may have similar characteristics relative to broadband instruments. But the OLR from global analyses can often differ from observations by more than 15 W m^{-2}; comparison with observations provides a useful measure of the quality of the OLR product. In this section we will use the *NOAA-12* OLR as the basis for comparison, then check the robustness of our results using OLR data from *NOAA-11*, which had different equatorial crossing times.

Figure 6a shows the time-mean *NOAA-12* OLR for December 1992. Figure 6b shows the difference between the NOAA OLR and OLR from the GEOS control sampled at the *NOAA-12* observation times. The corresponding differences for case A (with SSM/I rainfall) and case B (with SSM/I rainfall and TPW) are shown in Figs. 6c and 6d, respectively. Table 3 shows that assimilating SSM/I rain rates (case A) reduces the spatial bias in the monthly mean OLR by 6.4% and the error std dev by 13% between 20°S and 20°N. Assimilating SSM/I rain rates with TPW (case B) yields greater improvements, increasing the spatial anomaly correlation from 0.73 to 0.82 and reducing the bias by 46% and the error std dev by 26%. Overall, assimilating the SSM/I TPW without precipitation (case C) reduces most of the bias but not the error std dev, while assimilating SSM/I rain rates (case A) reduces the error std dev but not the bias. Only the simultaneous use of SSM/I rain rates and TPW gives the best result. The reason becomes clear when we examine the OLR in clear- and cloudy-sky regions separately.

When SSM/I rain rates and TPW are both assimilated, the improved OLR reflects (i) changes in cloud-sky regions as a result of improved precipitation and (ii) changes in clear-sky regions associated with reduced moisture biases in the lower troposphere. Figure 7 shows that a clear correspondence exists between the change in the monthly mean cloudy-sky OLR (case B minus control) and the change in precipitation (Fig. 5a), with a spatial anomaly correlation of −0.71 for the Tropics. Since the anomaly correlation between the cloudy-sky OLR change and the total OLR change (Fig. 5c) is 0.97, the improved OLR pattern in the Tropics reflects mostly the improved cloudy-sky OLR through rainfall assimilation.

By contrast, the improved clear-sky OLR can be directly linked to the reduced dry bias through TPW assimilation. Changes in the clear-sky OLR correspond to improved OLR in regions of large-scale subsidence over the eastern Indian Ocean off Australia, the eastern tropical Pacific, and the tropical Atlantic, outside the ITCZ. Figures 7b and 7c show that the correlation between the change in the clear-sky OLR and that in TPW is −0.87.

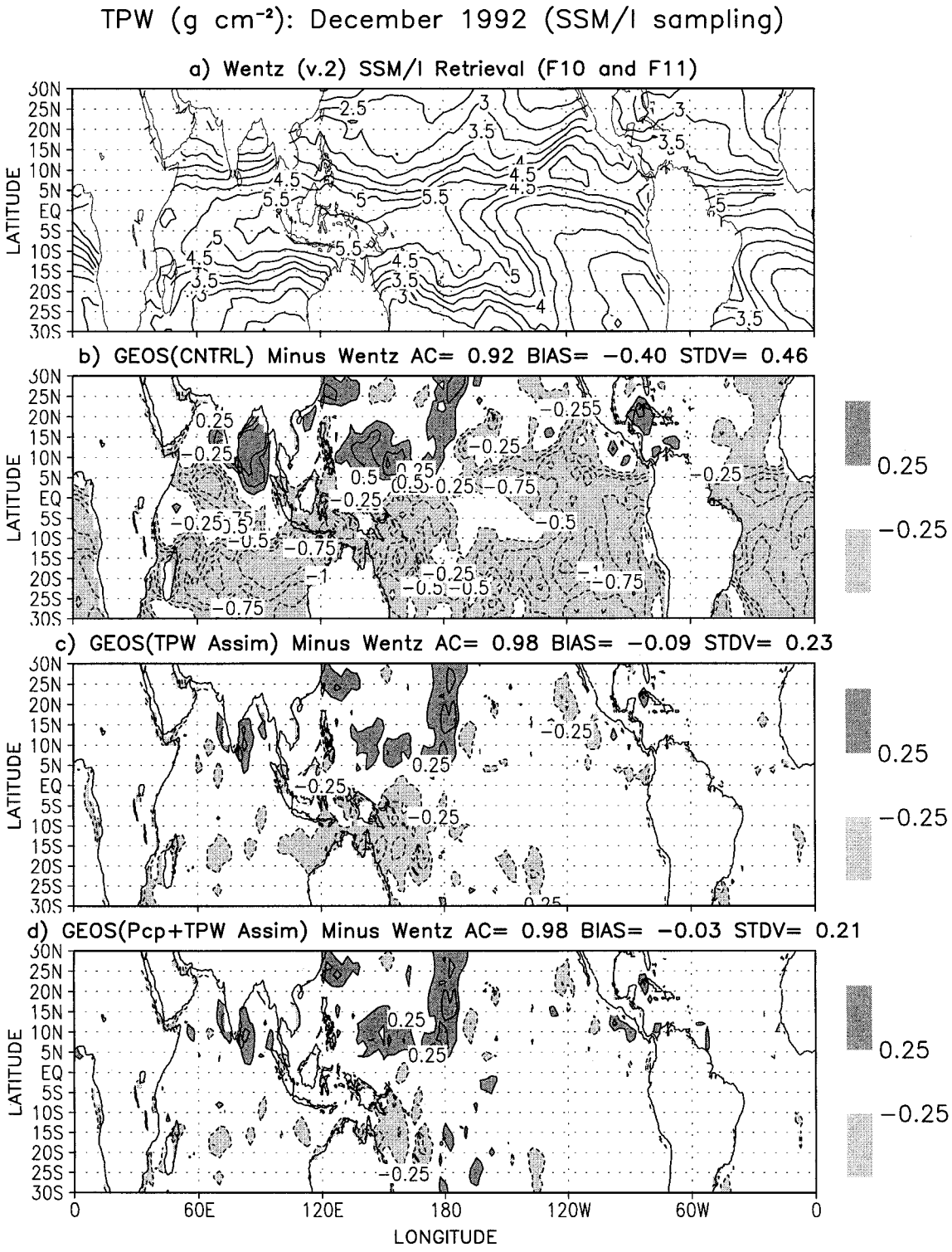

FIG. 4. (a) Time-mean SSM/I Wentz TPW estimate for Dec 1992. The contours are in increments of 0.5 g cm^{-2} from 1.5 g cm^{-2}. (b) Difference between SSM/I TPW and TPW from the control sampled at SSM/I observation locations. The contour interval is 0.25 g cm^{-2} with an additional contour at -2 g cm^{-2}. (c) Same as (b) but for case C. (d) Same as (b) but for case B.

TABLE 2. Spatial statistics of December-mean TPW minus SSM/I Wentz (version 2) retrieval 20°S–20°N and 30°S–30°N (in parentheses).

	Anomaly corr	Bias (g cm^{-2})		Error std dev (g cm^{-2})	
Control	0.89 (0.92)	−0.42 (−0.40)	— —	0.48 (0.46)	— —
Case C (TPW)	0.97 (0.98)	−0.10 (−0.09)	−76% (−78%)	0.24 (0.23)	−50.9% (−50.0%)
Case B (Pcp + TPW)	0.98 (0.98)	−0.03 (−0.03)	−93% (−93%)	0.22 (0.21)	−54.8% (−53.7%)
Case A (Pcp)	0.88 (0.91)	−0.28 (−0.31)	−33% (−23%)	0.54 (0.51)	+11.4% (+10.8%)

The above results are based on comparisons using daily mean values of OLR from *NOAA-12*. We repeated the comparisons using daily mean values from *NOAA-11*. The results are essentially the same, with the percentage reductions in the error std dev (Table 3) altered by only 1%. Our conclusions are therefore valid regardless of which NOAA satellite was used.

e. Reduction of state-dependent systematic errors in OLR

Since the radiative time constant and the overturning time of the large-scale circulation in the Tropics are on the order of weeks, it is conceivable that the quality of the analysis may continue to improve over an initial adjustment period from the time the SSM/I rainfall and TPW are first ingested. To investigate this, we examined the error std dev of the daily OLR for 30 days. Figure 8 shows that the error std dev reduction on day 30 is not greater than that on day 1, with no indication of errors decreasing with time. Figure 8 also shows that the error std dev decreases as the averaging period increases, consistent with reduced smaller random errors through time averaging. Note, however, that the offset in the error std dev in watts per square meter between case B and the control is comparable for all averaging periods. We interpret this to mean that SSM/I rainfall and TPW assimilation effectively reduces the systematic errors in the OLR. Moreover, this systematic error reduction is likely a function of the state since errors in the std dev pertain to spatially varying, state-dependent fields, with the state-independent error already accounted for in the bias. When a longer assimilation becomes available, it may be possible to identify through EOF analysis coherent low-frequency spatial patterns associated with this error std dev reduction.

With the error std dev decreasing with the time-averaging length, a constant error std dev reduction for different averaging periods corresponds to a larger *fractional* error reduction for longer averaging periods. The fractional error std dev reduction in the 30-day mean OLR averaged from 20°S to 20°N is about 26%, nearly twice the fractional error reduction in daily mean OLR. A similar diparity in fractional error reduction between the monthly mean field and the daily mean fields is to a lesser extent also evident in precipitation. Based on this we conclude that while the rainfall and TPW assimilation improves the 6-h analysis, it is even more effective in improving the monthly averaged assimilation fields. Clearly, the full benefit of assimilating these data types cannot be gauged solely in terms of their impact on the 6-h assimilation cycle.

f. Comparison with ISCCP cloud data

We have shown in section 4d that the reduced error std dev of OLR is due mainly to changes in the cloudy-sky OLR. Since the anomaly correlation between the monthly mean total cloud fraction and the cloudy-sky OLR (Fig. 7a) is −0.58, the improved cloud-sky OLR implies improved cloud fraction in the assimilation. For this period, the ISCCP D1 cloud data are available from the NASA/Langley Distributed Active Archive Center. The ISCCP cloud fraction product, despite the lack of absolute validation, is expected to contain useful spatial information. Although the definition of cloudy sky in satellite observation differs from that used for gridded model data, a comparison with the ISCCP cloud fraction data may still be meaningful if the differences are large. The statistics in Table 4 show the effect of rainfall and TPW assimilation on the total cloud fraction. Given the uncertainty of the observations, it is questionable whether spatial biases on the order of 0.1 are meaningful. But reductions of 5%–10% in the error std dev are statistically significant at the 95% level according to the F test. These improvements, though modest, are consistent with the improved OLR in cloudy-sky regions. It is possible that we may find greater improvements in the high-cloud fraction, which is more closely linked to the cloudy-sky OLR; unfortunately, high-cloud fraction was not generated as a diagnostic in the GEOS DAS.

g. Shortwave radiation at the surface

Another test of possible improvements in clouds is to see if there is evidence of improved shortwave radiation at the surface. In this section we compare the net shortwave flux at the surface from the assimilation with Pinker's 3-h average combined satellite–model es-

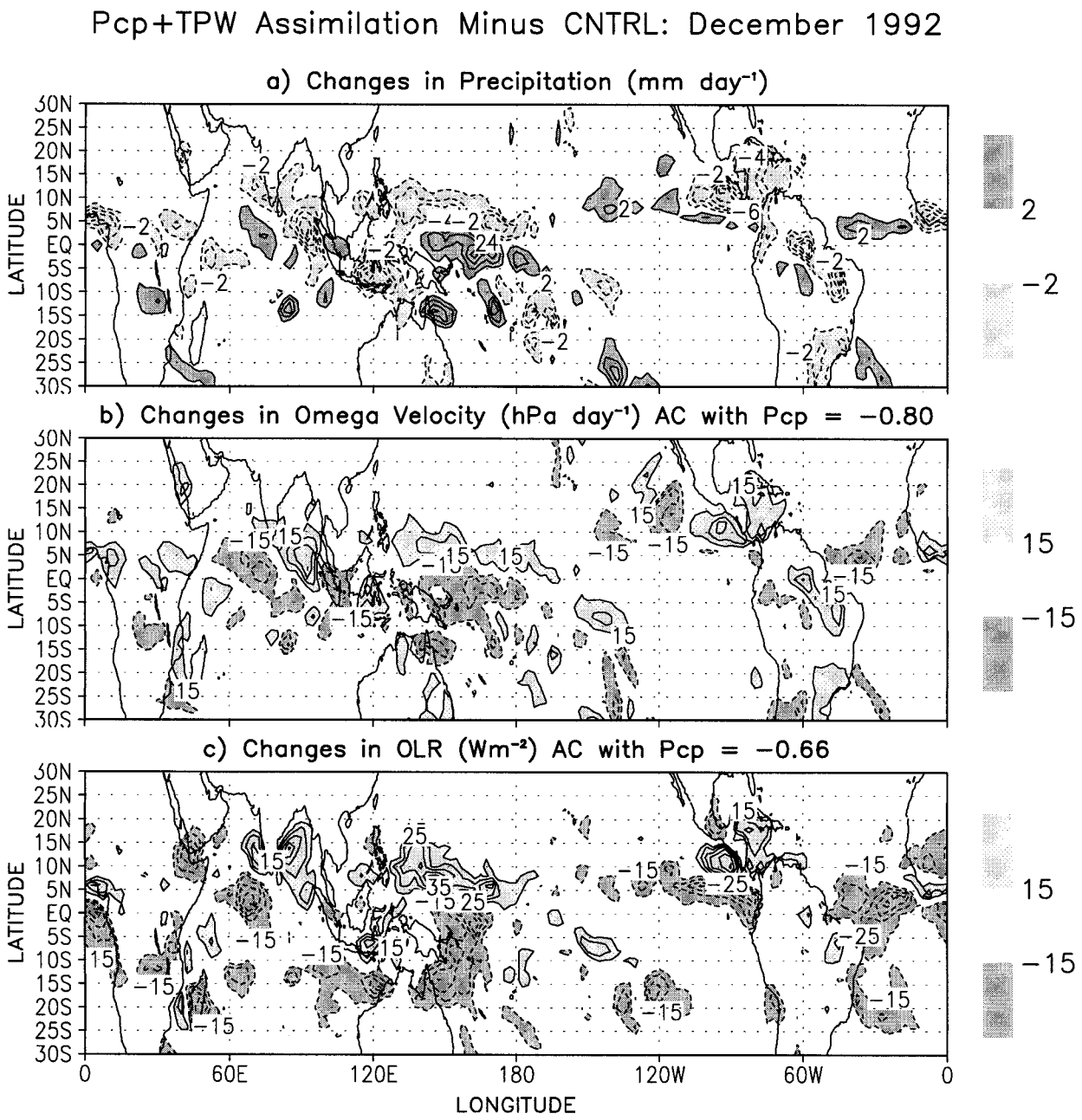

FIG. 5. (a) Difference in monthly mean precipitation between case B and the control for Dec 1992. The contour interval is 2 mm day^{-1}. (b) The corresponding difference in the omega velocity at 500 hPa. The contour interval is 20 hPa day^{-1}. The correlation between this and the change in the precipitation pattern is −0.80. (c) The corresponding change in OLR. The contour interval is 10 W m^{-2}. The correlation between this and the change in precipitation is −0.66.

timate using ISCCP D1 cloud data (R. T. Pinker 1998, personal communication). The basic methodology for computing the shortwave flux using ISCCP cloud data is given in Pinker and Lazlo (1992). Figure 9 shows the difference in the net downward shortwave radiative flux at the surface between Pinker's estimate and those from three assimilation runs. The GEOS DAS is known to underestimate the cloud amount over continents and overestimate clouds over large areas over oceans. Rainfall and TPW assimilation improves the surface shortwave fluxes over both land and oceans. Table 5 shows that assimilating SSM/I rain rates with or without the TPW data reduces both spatial biases and error std dev in the Tropics. These results provide further evidence that use of SSM/I rainfall data helps improve clouds in the assimilation. However, assimilating SSM/I TPW data without rain rates (case C) seems to degrade the shortwave flux at the surface.

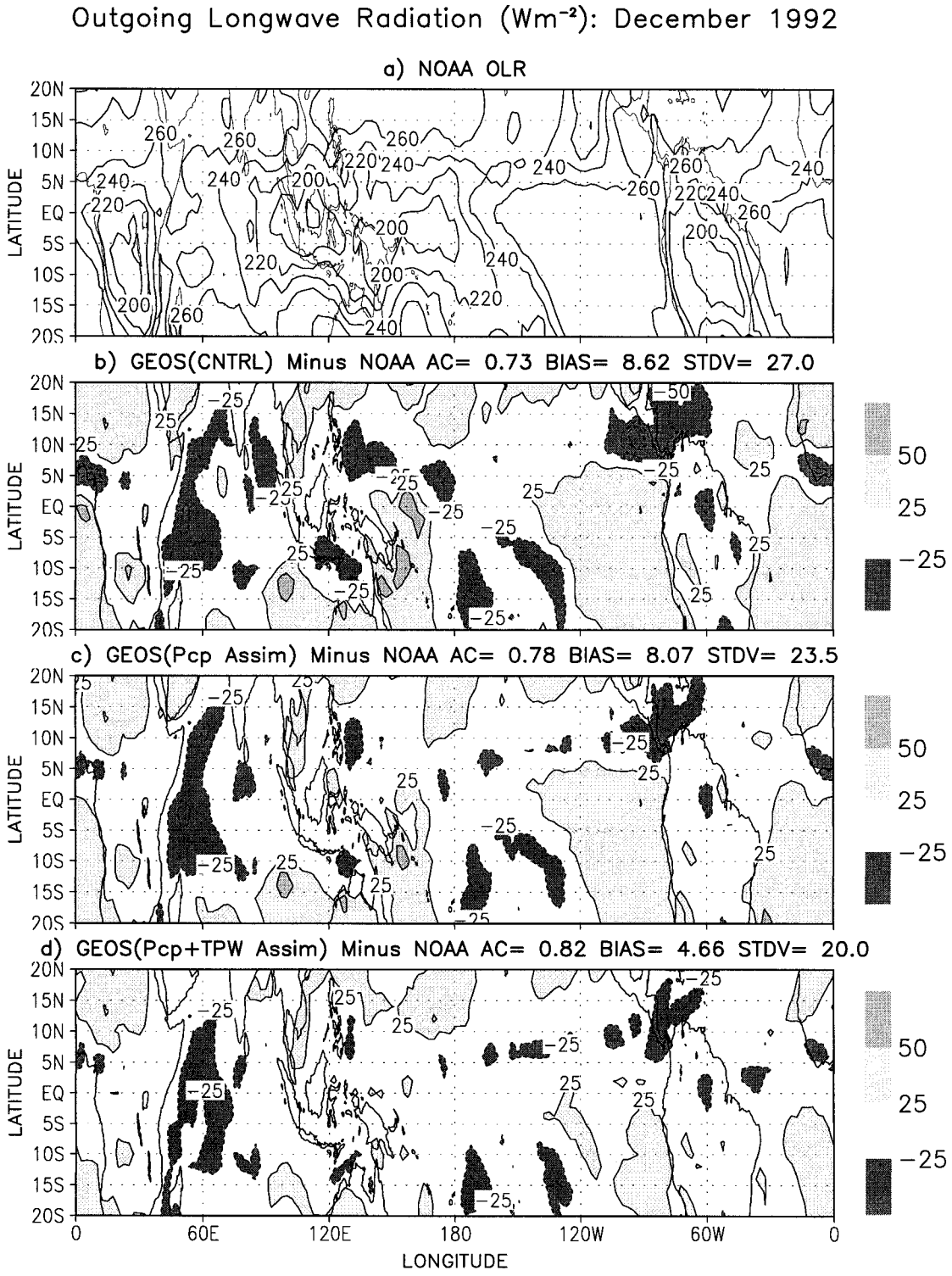

FIG. 6. (a) Time-averaged AVHRR OLR from *NOAA-12* for Dec 1992. The contour interval is 20 W m^{-2}. (b) Difference between NOAA OLR and OLR from the control with the same sampling. The contour interval is 25 W m^{-2}. (c) Same as (b) but for case A. (d) Same as (b) but for case B.

TABLE 3. Spatial statistics of December-mean OLR minus *NOAA-12* OLR estimate 20°S–20°N and 30°S–30°N (in parentheses).

	Anomaly corr	Bias (W m^{-2})		Error std dev (W m^{-2})	
Control	0.73	8.62	—	27.0	—
	(0.74)	(13.5)	—	(24.8)	—
Case A (Pcp)	0.78	8.07	−6.4%	23.5	−13.0%
	(0.78)	(13.4)	(−0.7%)	(22.4)	(−10.0%)
Case B (Pcp + TPW)	0.82	4.66	−46%	20.0	−26.0%
	(0.81)	(9.5)	(−30%)	(19.6)	(−21.1%)
Case C (TPW)	0.77	1.61	−81%	26.8	−0.90%
	(0.76)	(7.35)	(−46%)	(25.3)	(+1.8%)

5. Impact on forecast

The view that improvements to the analysis can be evaluated in terms of the forecast it produces rests on the assumption that the model is perfect. In reality the forecast model is not perfect. The analysis scheme must take into account both observation and model errors to arrive at an optimal estimate of the climate state. In previous sections we have shown that rainfall and TPW assimilation improves the time-averaged fields more than the 6-h analysis, suggesting that improvements in the instantaneous fields may have only a small impact on the model forecast. But internal consistency between model physics and observations requires that there still be some improvement, or, at least, no degradation, in the short-term forecast made from an improved climate dataset. In this section we examine the impact of rainfall and TPW assimilation on model forecasts in terms of the 6-h observation minus forecast (O–F) residuals as well as 5-day forecasts.

a. Observation minus forecast residual

Table 6 shows 6-h averaged O–F residuals for precipitation for lead times from 6 to 48 h averaged over all tropical locations with available SSM/I rain rates. The forecasts were obtained using initial conditions that were 1 day apart over a 10-day period. These were treated as independent samples since convective precipitation has a lifetime on the order of hours. Bias and error std dev differences significant at the 99% level are italicized in Table 6. They show that precipitation forecasts in case B have smaller error std dev within the first 12 h, reflecting reduction of errors in the initial conditions; but the magnitudes of error reduction are less than 7% percent, much less than the 32%–40% reductions in the 6-h assimilation (section 4a). This shows that assimilating these data types can improve the analysis as a climate dataset without necessarily achieving comparable improvements in the first guess (i.e., the 6-h forecast). Table 6 also shows that even though biases are much smaller than the error std dev in precipitation forecasts, rainfall and TPW assimilation can reduce the bias relative to the SSM/I rain rate by 40% in forecasts beyond 1 day. Although the overall improvement of the precipitation forecast is modest, it is significant that assimilating these data types does not degrade the short-range forecast while improving the time-mean analysis, as expected of a physically consistent assimilation system.

Figure 10 compares the monthly mean biases and standard deviations of the 6-h O–F residuals for winds, geopotential height, and specific humidity averaged over tropical rawinsonde locations for case B and the control. Statistical tests show that only changes in the O–Fs for moisture are significant. Probabilities from Student's *t*-test indicate larger moisture biases (at the 1% level) in case B between 400 and 700 hPa. However, the standard deviations in the two assimilations are different between 400 and 500 hPa according to the F test, casting doubt on the soundness of the *t*-test at these levels (see Table 7). But, the overall indication is that rainfall and TPW assimilation may have moistened the upper-level humidity in the Tropics. This issue is further investigated in section 6. We obtained similar results for case A with no TPW observations.

b. Ensemble 5-day forecast

We examined the impact of SSM/I rainfall and TPW assimilation on an ensemble of 5-day forecasts with initial conditions 5 days apart. With 1 month of assimilation, the ensemble size of the 5-day forecast is limited to six cases. The uncertainty associated with such a small sample can be large, we relied on Student's *t*-test to detect differences in the ensemble means under conditions where the standard deviations of the ensembles being compared are the same according to the F test.

Figure 11 compares the ensemble forecasts of the tropical geopotential height at 500 hPa with initial conditions taken from the GEOS control and case B assimilations. For forecast verification, we use two analyses: the operational analysis from the European Centre for Medium-Range Weather Forecasts (ECMWF) and the GEOS analysis from case B, which has smaller errors compared with satellite observations in the Tropics, as shown in section 4. Figure 11 shows ensemble-mean forecast rms error and error std dev for the first 5 days. Assimilation of SSM/I rainfall and TPW data yields

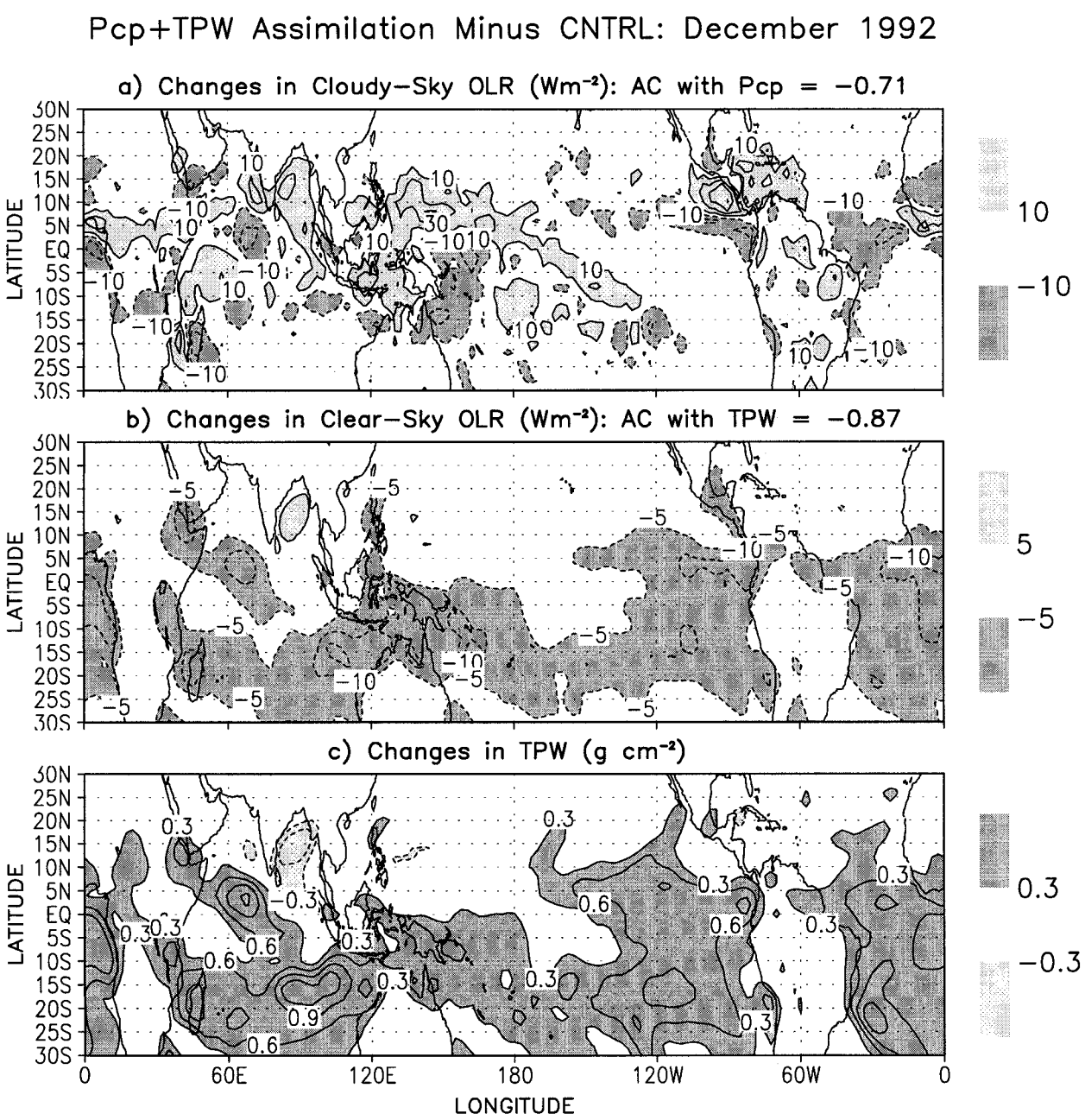

FIG. 7. (a) Difference in the cloudy-sky OLR between case B and the control for Dec 1992. The contour interval is 20 W m^{-2}. The correlation between this and the change in precipitation (Fig. 5a) is −0.71. (b) Difference between the clear-sky OLR in case B and the control for the same period. The contour interval is 5 W m^{-2}. (c) The corresponding change in TPW. The contour interval is 0.3 g cm^{-2}. The correlation between this and the change in the clear-sky OLR is −0.87.

smaller rms errors in the tropical height forecast regardless of whether the ECMWF or the GEOS analysis is used for verification. Results of F tests show that the two forecast ensembles (with the same verification analysis) have standard deviations that are statistically indistinguishable, thus permitting Student's *t*-test despite the small sample size. Results show significant rms error reductions at the 95% level between 1.5 and 3 days with the ECMWF analysis as the verification, compared with significant improvements between 0.5 and 4 days with the GEOS analysis as the verification.

Rainfall and TPW assimilation does not improve nor degrade the 5-day forecast in the extratropics. The ensemble-mean forecast anomaly correlations shown in Fig. 12 are not statistically different. This again demonstrates that the improved time-averaged assimilation fields shown in section 4 were not achieved at the expense of forecast skills.

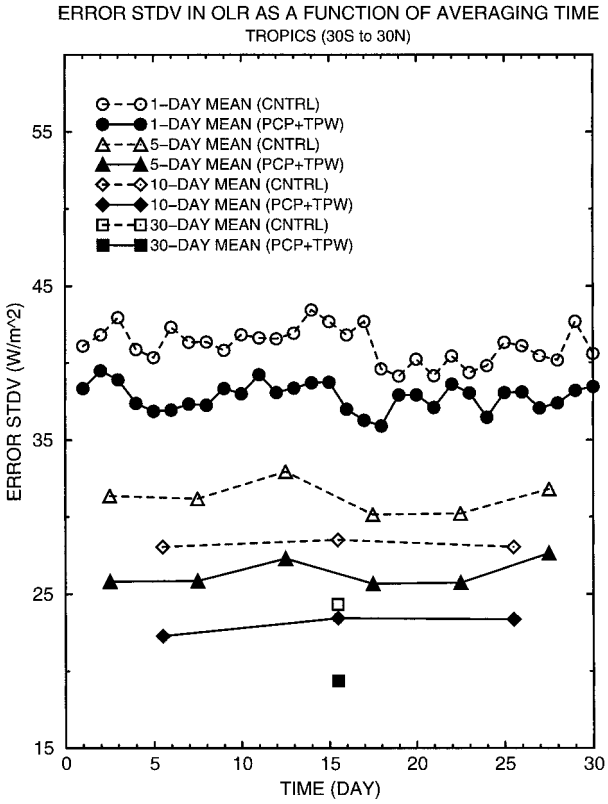

FIG. 8. Error std dev in tropical OLR in case B as a function of averaging periods of 1, 5, 10, and 30 days. Results are for the first 30 days in Dec 1992, with data points at the middle of their averaging periods.

6. Comparison of synthetic radiances with TOVS measurements

In this section we use TOVS brightness temperature observations to examine the impact of the rainfall assimilation on upper-tropospheric humidity and tropospheric temperature. We first compute brightness temperatures using temperature and humidity fields from the control and precipitation assimilations (referred to as synthetic brightness temperatures). We then compare the synthetic brightness temperatures with observed brightness temperatures. We will refer to the difference between observed and synthetic brightness temperatures as residuals.

The observations consist of clear and cloud-cleared infrared radiances from the TOVS High-Resolution Infrared Radiation Sounder 2 (HIRS2) and brightness temperatures from the TOVS Microwave Sounding Unit (MSU). Most of the HIRS2 radiance observations have been processed to remove the effect of cloud (a process referred to as cloud clearing). The HIRS2 clear and cloud-cleared radiances are then converted to equivalent blackbody (brightness) temperatures. The HIRS cloud-cleared brightness temperatures were produced as part of the Pathfinder Path A dataset (Susskind et al. 1997). The cloud-clearing approach is based on Susskind et al. (1984). The only adjustment to the HIRS2 clear-scene brightness temperature is averaging of two or more adjacent pixels. The MSU brightness temperatures are not adjusted in any way (e.g., no adjustment to nadir view, etc.). Brightness temperatures are computed at the observed satellite zenith angle.

The radiative transfer algorithm used to compute brightness temperatures is a fast transmittance model based on Susskind et al. (1983) with the interface of Sienkiewicz (1996). The inputs are temperature and humidity profiles from the surface to 0.4 hPa, the surface skin temperature, and microwave emissivity (the infrared surface emissivity is fixed at the values used in the Pathfinder processing). In the brightness temperature calculation, we use the surface skin temperature and microwave emissivity from the Pathfinder dataset. The temperature and humidity profiles are from the different assimilation runs and are interpolated linearly in space (not in time) to observation locations for a given 6-h assimilation cycle.

Both the observations and radiative transfer calculation contain biases. We estimate the absolute uncertainty of the synthetic minus observed brightness temperatures to be approximately 2 K. We have not made any attempt to remove these biases. Instead, we concentrate on the spatial structure of the residuals, cases where the overall bias between observations and synthetic brightness temperatures exceeds 2 K, and the relative differences between the control and precipitation assimilations.

TABLE 4. Spatial statistics of December-mean total cloud fraction minus ISCCP D1 estimate 20°S–20°N and 30°S–30°N (in parentheses).

	Anomaly corr	Bias	Error std dev	Std dev change
Control	0.46 (0.45)	0.112 (0.060)	0.217 (0.231)	— —
Case A (Pcp)	0.41 (0.41)	0.129 (0.075)	0.203 (0.226)	−2.0% (−2.3%)*
Case B (Pcp + TPW)	0.47 (0.44)	0.163 (0.117)	0.186 (0.212)	−10.1% (−8.2%)
Case C (TPW)	0.51 (0.47)	0.140 (0.087)	0.197 (0.226)	−4.8% (−2.2%)*

* The change is not statistically significant (with a probability exceeding 0.05 by the F test).

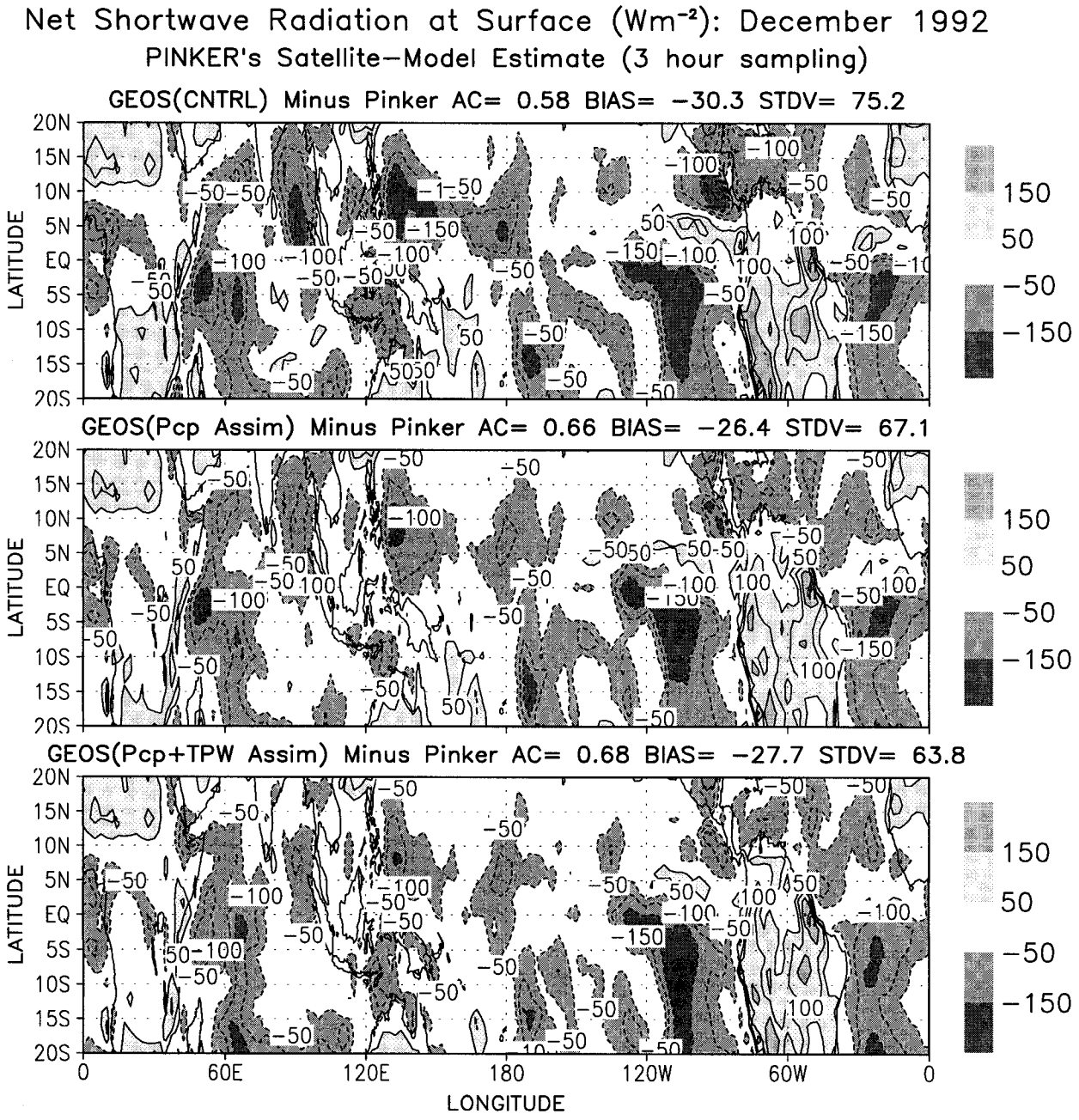

FIG. 9. (a) Difference in the net downward shortwave radiation at the surface between the control and Pinker's satellite–model estimate for Dec 1992. The comparison is based on 3-h sampling of ISCCP clouds. The contour interval is 50 W m^{-2}. (b) Same as (a) but for case A. (c) Same as (a) but for case B.

We examine in particular two channels from the TOVS instruments, namely, HIRS2 12 (6.7 μm), which is sensitive to upper-tropospheric humidity (UTH) and MSU 2, which is sensitive to tropospheric temperature. HIRS2 12 has a peak sensitivity to UTH between about 300 and 500 hPa depending on local conditions. MSU 2 has a relatively broad sensitivity to tropospheric temperature that peaks near 600 hPa. It reaches half its peak sensitivity at approximately 300 hPa and has a small sensitivity to surface emission. The effect of nonprecipitating cloud on MSU 2 is negligible in most cases and therefore is not accounted for. Precipitating situations are screened out by checking for inconsistencies between microwave and infrared observation and checking high values of the microwave emissivity over ocean.

Figure 13 compares the monthly mean synthetic HIRS2 12 brightness temperature of the control and that

TABLE 5. Spatial statistics of December-mean surface shortwave flux minus Pinker's satellite–model estimate 20°S–20°N and 30°S–30°N (in parentheses).

	Anomaly corr	Bias (W m^{-2})		Error std dev (W m^{-2})	
Control	0.58 (0.71)	−30.3 (−22.5)	— —	75.2 (73.0)	— —
Case A (Pcp)	0.66 (0.76)	−26.4 (−19.0)	−13% (−16%)	67.1 (67.1)	−10.8% (−8.1%)
Case B (Pcp + TPW)	0.68 (0.77)	−27.7 (−21.9)	−8.5% (−2.7%)	63.8 (65.5)	−15.1% (−10.3%)
Case C (TPW)	0.60 (0.71)	−44.5 (−34.6)	+47% (+53%)	72.6 (72.8)	−3.5% (−0.4%)*

* The change is not statistically significant (with a probability exceeding 0.05 by the F test).

in case A with observation. We obtained similar results for HIRS2 11 (7.3 μm), which is also sensitive to humidity but peaks at a lower altitude than HIRS2 12. Figure 13a shows that the brightness temperature of the control has a cold bias, implying a moist bias in UTH. Figure 13b shows that the UTH averaged over the Tropics in case A has a stronger bias and a slightly larger error std dev. The rainfall assimilation scheme in its current implementation thus has an overall negative impact on UTH. However, a difference plot of the synthetic radiances (Fig. 13c) shows that the brightness temperature in case A is warmer over much of the Tropics, typically away from areas of precipitation changes (Fig. 13d). This suggests that precipitation assimilation has improved the large-scale vertical motion field in the surrounding regions. The warmer brightness temperatures likely reflect a drying of the upper troposphere through a stronger subsidence. But this improvement is offset by excessive local moistening in areas of reduced precipitation when averaged over the Tropics (see the error statistics in Figs. 13a and 13b). This is consistent with that the rms error of the brightness temperature averaged over the Tropics excluding areas of reduced rain rates is 3.24 K in case A compared with 3.28 K in the control.

The negative impact on UTH at locations of reduced precipitation is a direct consequence of the 1D linear slope adjustment of relative humidity, as shown in Fig. 1b. The scheme may be modified to concentrate the adjustment near the surface to alter the conditional instability, or incorporate additional vertical structure information if available. We are currently testing an alternative α profile based on the Jacobian of the cost function $J(\Delta q)$ that effectively confines the Δq to near the surface. The results will be reported in a subsequent paper.

The impact of rainfall assimilation on the tropospheric temperature may be inferred from Fig. 14, which shows the monthly mean synthetic MSU 2 brightness temperatures in the control and case A are both higher than the observed MSU 2 values (Fig. 14a), suggesting that analyzed temperatures may be too warm. But these differences in brightness temperatures may not be significant given that the overall uncertainty is about 2 K. We can remove this ambiguity by examining changes in the synthetic radiances between case A and the control. Figure 14c shows the impact of rainfall assimilation is to reduce possible warm biases by about 0.1 K in regions where rain rates have been modified (see Fig. 13d). A change of 0.1 K may be significant given the broad weighting function and is consistent with that the error std dev is also reduced. In any case, there is no

TABLE 6. Observation minus forecast statistics for precipitation in the Tropics.

Forecast time	6 h	12 h	18 h	24 h	30 h	36 h	42 h	48 h
Sample size	25 043	24 233	26 339	26 267	2690	27 250	27 786	26 898
				Bias				
Control	−0.21	−0.33	−0.48	−1.12	−0.68	−0.75	−0.89	−1.27
Case B	−0.31	−0.38	−0.36	−0.88	−0.41	−0.44	−0.53	−0.84
% change	47.6%	15.5%	−25.0%	−21.4%	*−39.7%*	*−41.3%*	*−40.4%*	*−33.8%*
T-test prob	0.4	0.6	0.3	0.07	*0.01*	*0.006*	*0.001*	*0.0008*
				Error std dev				
Control	15.05	14.25	14.03	15.98	12.50	13.39	13.25	15.23
Case B	14.08	13.78	14.00	15.96	12.45	13.38	13.29	15.26
% change	*−6.4%*	*−3.3%*	*−0.2%*	−0.1%	−0.4%	−0.07%	0.3%	0.1%
F-test prob	*0.0*	*1×10^{-7}*	*0.7*	0.8	0.5	0.9	0.6	0.7

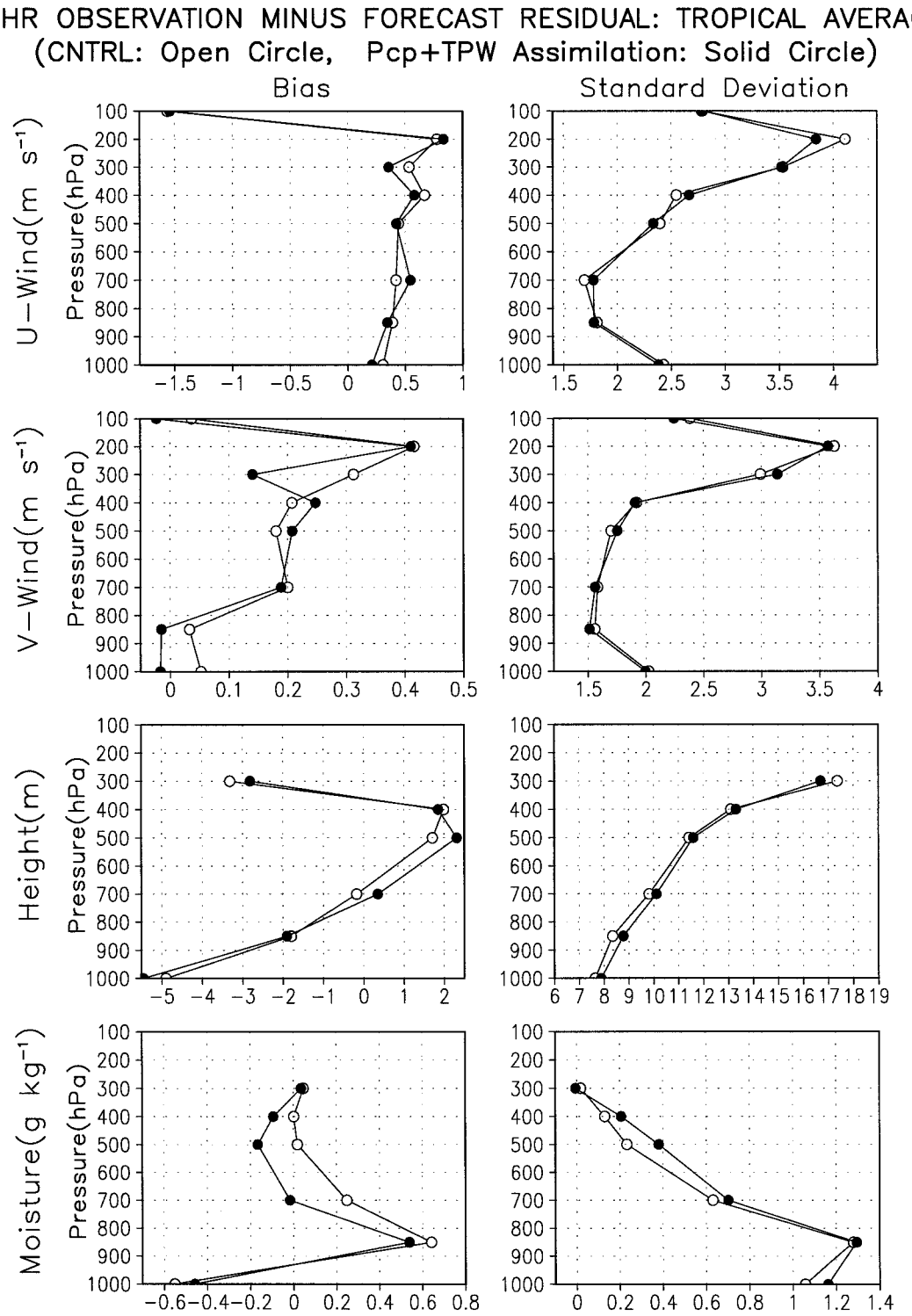

FIG. 10. Monthly averaged biases and standard deviations of 6-h O–F residuals for winds, geopotential height, and specific humidity averaged over the Tropics for Dec 1992: Open circles for the control. Solid circles for case B.

TABLE 7. Probability of the December-mean tropical O–F residual for specific humidity being the same in case B and the control.

Pressure (hPa)	T-test probability for bias	F-test probability for std dev
300	0.150 112 2	1.438×10^{-4}
400	3.846×10^{-8}	9.398×10^{-7}
500	1.734×10^{-12}	5.292×10^{-11}
700	3.888×10^{-8}	0.099 4
850	0.245 183 2	0.855 3
1000	0.405 889 2	0.306 0

evidence of rainfall assimilation adversely affecting the tropospheric temperature.

7. Sensitivity to SSM/I-derived precipitation intensity

In this section we test the sensitivity of our results to the SSM/I-derived rainfall intensity since there is still uncertainty in this quantity. At the present time, rain rates given by the various microwave retrieval algorithms may differ by as much as a factor of 2, while there is considerable agreement in terms of rainfall patterns (Adler et al. 1996). For physical initialization, Krishnamurti et al. (1994) found that the impact of rainfall assimilation on the model forecast is sensitive to the SSM/I-derived rain rate, which may reflect incompatibilities between the retrieved rain rates and the model's physical parameterizations. We do not expect to see this type of sensitivity in our 1+1D assimilation scheme within the IAU framework since the IAU tendencies would compensate for deficiencies in the model physics (whatever they might be). We tested this in an assimilation experiment in which the observed rain rate was 50% of the SSM/I GPROF retrieval and no TPW observation was used (as in case A). The observed tropical-mean precipitation in this case is about 1.5 mm day^{-1}, much smaller than the model estimate of 3 mm day^{-1} in the control. This experiment is a severe test of our algorithm's ability to assimilate such extreme rain rates and will reveal if the improved OLR in case A is due to improvements in the spatial pattern or intensity of the tropical rainfall.

Figure 15 shows that the 1+1D assimilation algorithm has no difficulty in assimilating these extreme rain rates, which increases the correlation with the observations from 0.53 to 0.80, and reduces the monthly mean bias by 62% and the error std dev by 47%. Figure 16 shows the impact on the December-mean OLR. Comparing Fig. 16 with Fig. 6c (with the SSM/I GPROF rain rate at its full strength) shows only minor differences. This confirms that improvement in the OLR through rainfall assimilation is due primarily to the improved spatial pattern of rainfall and is not sensitive to the retrieved rainfall intensity.

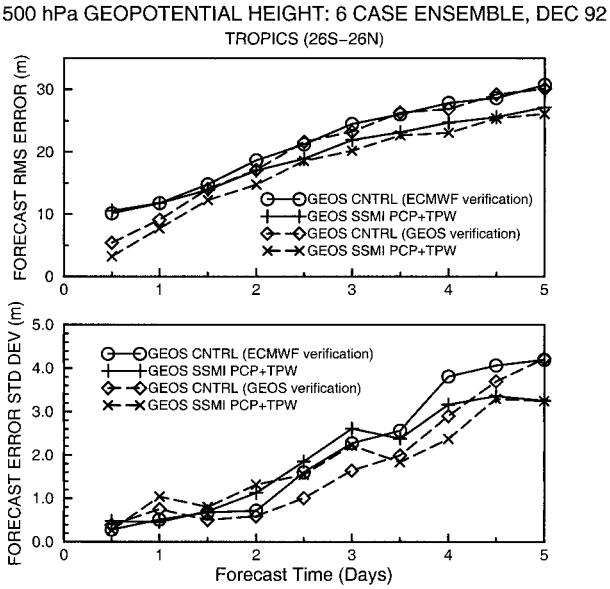

FIG. 11. Ensemble-mean rms error and error std dev for six cases of 5-day forecasts of the tropical geopotential height at 500 hPa: Solid lines are results using the ECMWF analysis as verification. Dashes are the same forecasts with the GEOS (case B) assimilation as verification.

8. Summary and discussion

We have developed a variational framework for assimilating 6-h averaged tropical precipitation and TPW estimates in the GEOS DAS and tested a simplified moisture-adjustment procedure in the limit of small ob-

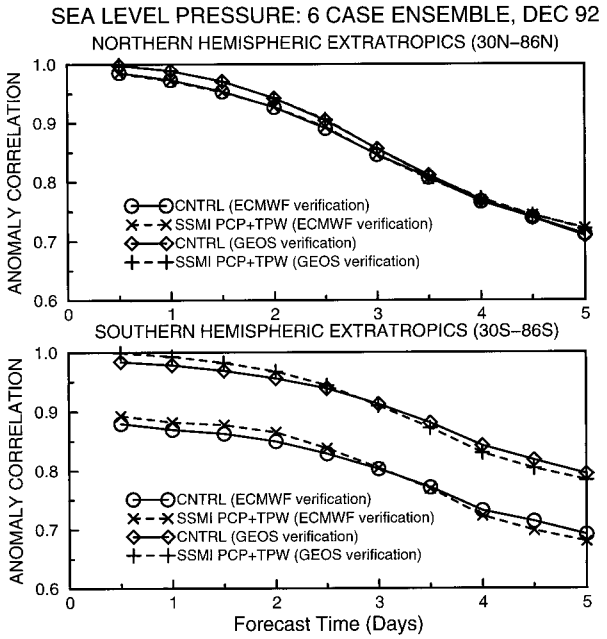

FIG. 12. Anomaly correlations of the sea level pressure for a six-case ensemble of 5-day forecasts: Solid lines for the control. Dashes for case B.

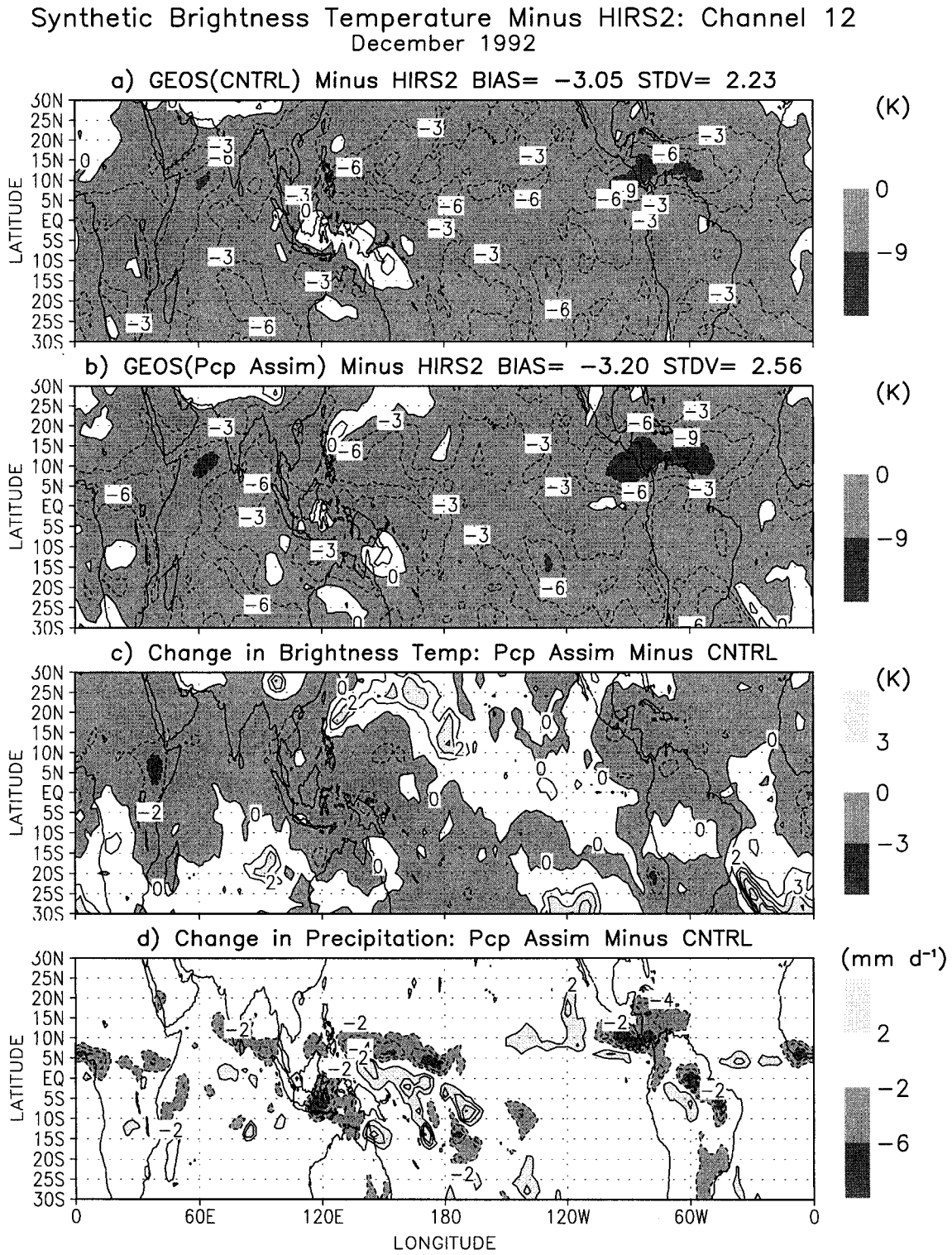

FIG. 13. Synthetic HIRS2 channel 12 brightness temperature for Dec 1992. (a) Control minus TOVS observation. (b) Case A minus TOVS observation. (c) Case A minus the control. (d) Corresponding change in precipitation for the same period.

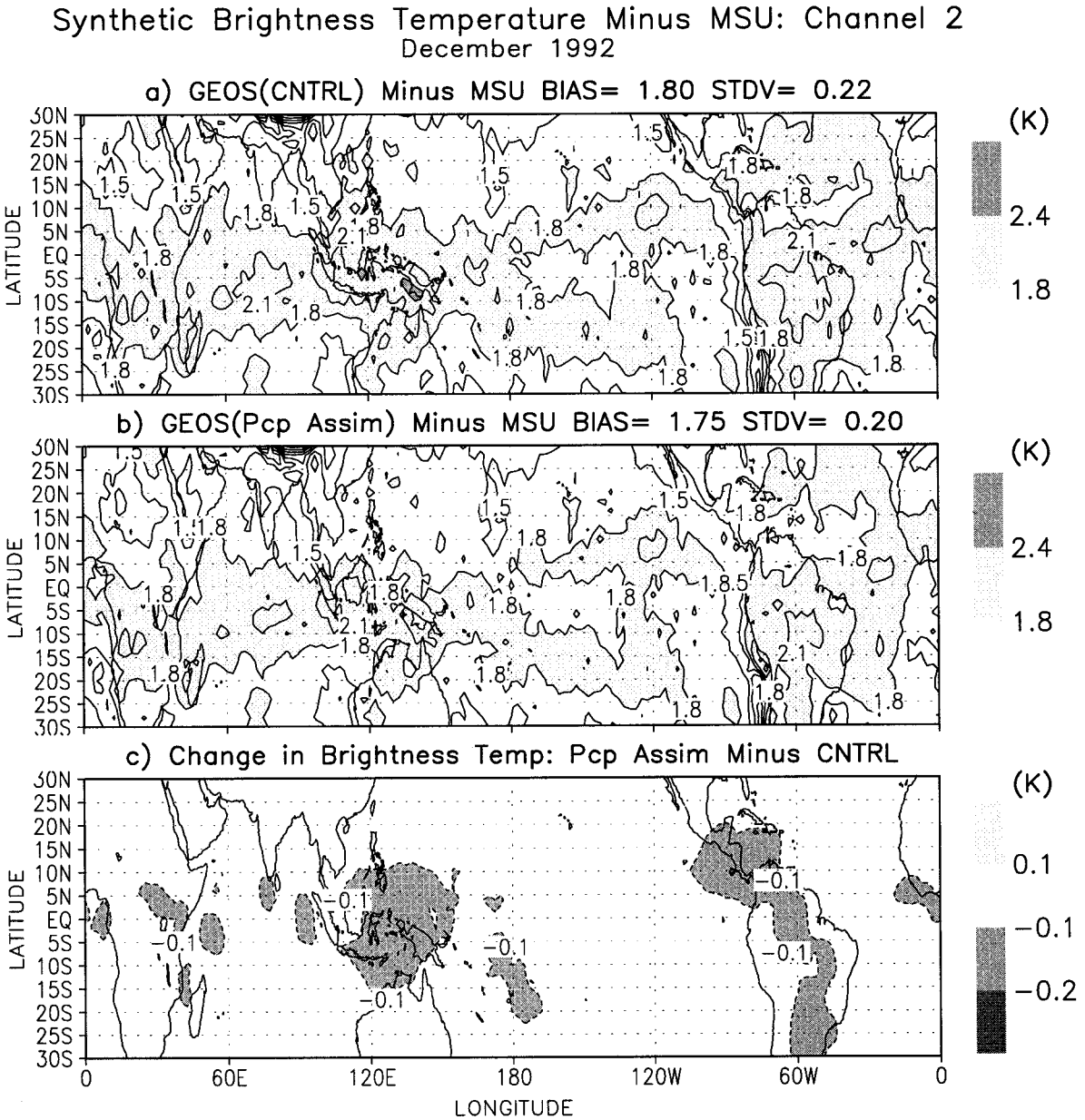

FIG. 14. Same as Fig. 13 except for the MSU channel 2.

servation errors. Results show that assimilating these data types not only improves precipitation and TPW in the analysis but also reduces biases and state-dependent systematic errors in fields such as OLR, clouds, surface radiation, and the large-scale circulation. Assimilating these data also improves the short-range forecast in the Tropics. The improvement in forecast is, however, modest, consistent with the fact that random errors can dominate over systematic errors in the instantaneous fields. An important result of this study is that improving the short-range forecast is not necessarily a prerequisite for improving the 4D assimilation as a climate dataset. In the presence of biases and other errors in the forecast model, it is possible to improve the time-averaged climate content of the analysis without equally significant improvements in forecast. The full benefit of rainfall and TPW assimilation cannot be gauged strictly in terms of forecast skills or the 6-h analysis.

Diagnostics show that assimilating SSM/I GPROF rain rates derived from the DMSP *F10* and *F11* satellites improves the spatial and temporal distributions of clouds and radiative fluxes in cloudy-sky regions, while assimilating SSM/I TPW retrievals reduces low-level moisture biases to improve the clear-sky longwave radiation in the analysis. In our case study for December 1992, using both data types leads to a 46% reduction in the

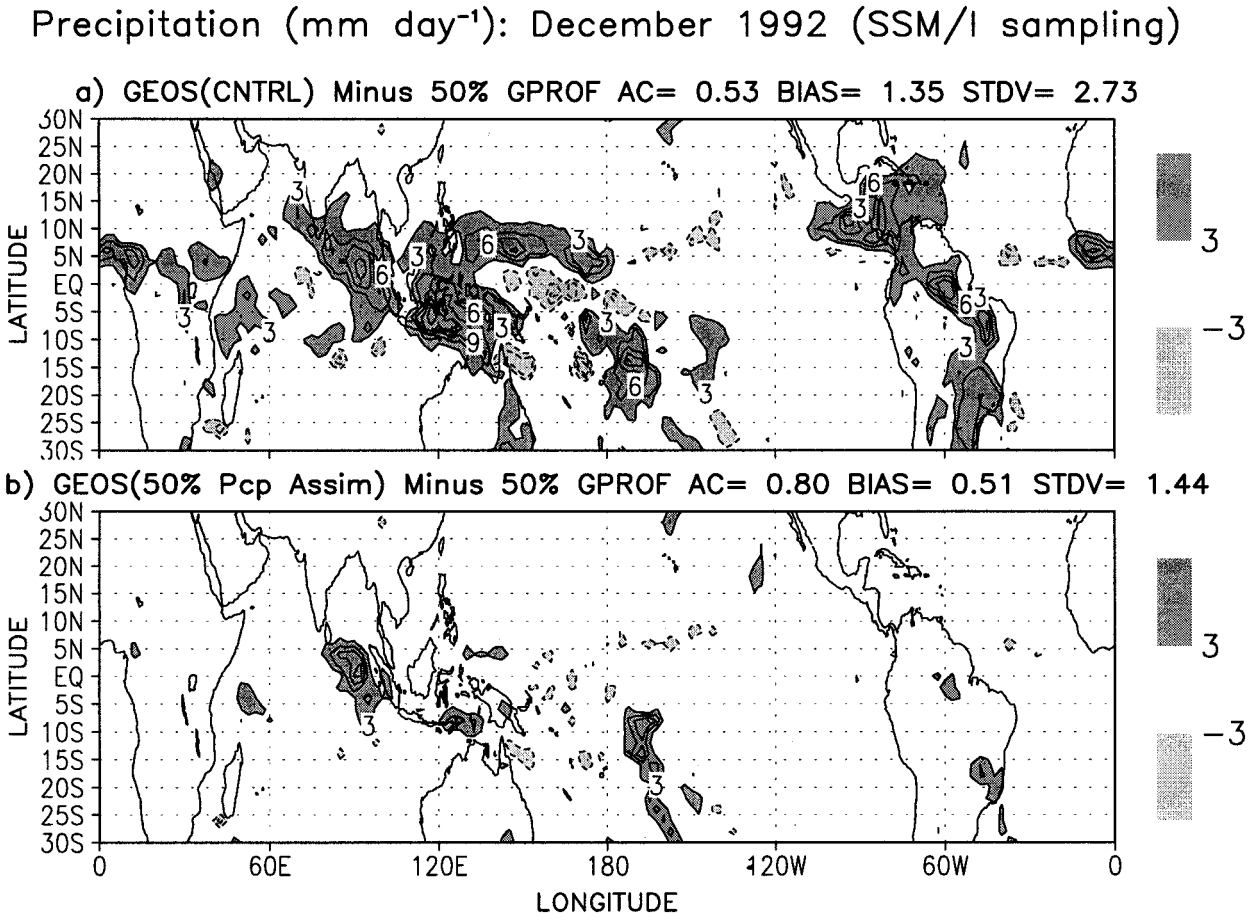

FIG. 15. Impact of rainfall assimilation on precipitation with the observed rain rate assumed to be 50% of the SSM/I GPROF rain rate. (a) Difference between the observed rain rate and precipitation from the control sampled at SSM/I observation locations. The contour interval is 3 mm day^{-1}. (b) Same as (a) but for precipitation assimilation.

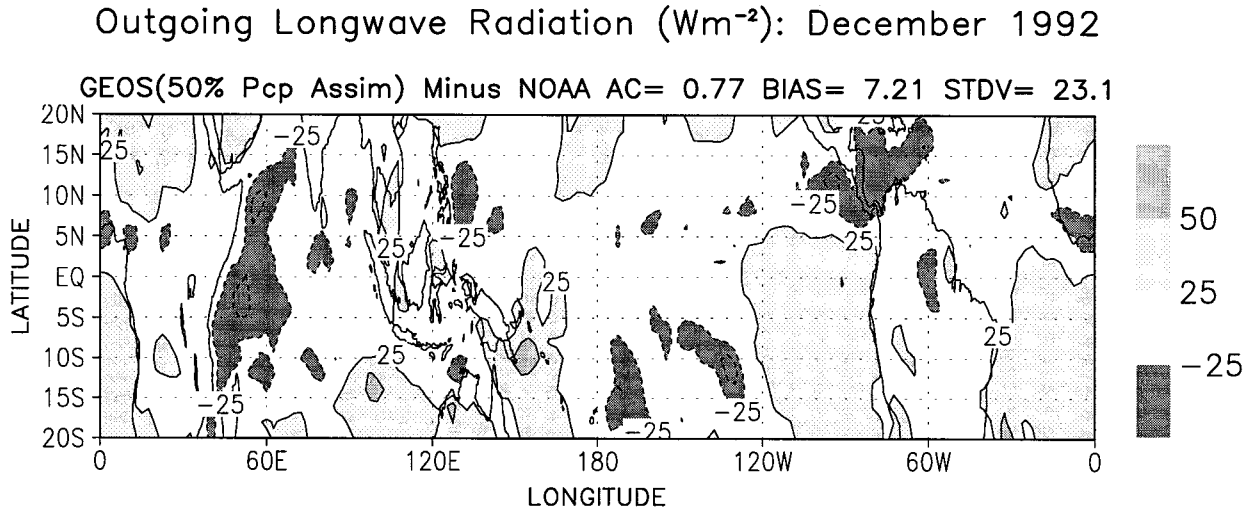

FIG. 16. Difference between NOAA OLR and OLR from the sensitivity experiment assimilating 50% of the SSM/I GPROF rain rate. The contour interval is 25 W m^{-2}.

spatial bias and 26% reduction in the error std dev in the monthly mean OLR averaged between 20°S and 20°N relative to NOAA OLR measurements. Comparisons with the ISCCP cloud data suggest that assimilating the SSM/I rain rates and TPW reduces the monthly mean error std dev in the total cloud fraction. This is consistent with the reduced spatial bias and error std dev in the monthly mean shortwave radiation at the surface, compared with Pinker's satellite–model estimate.

By improving the latent heating distribution, rainfall assimilation should improve the large-scale circulation in the Tropics, which is difficult to verify given the sparse wind observations in the Tropics. There are, however, indirect measures of the effect of rainfall assimilation on the vertical motion field (and, by association, the related horizontal divergent motions). In regions away from detraining clouds, sinking motions reduce the upper-tropospheric humidity through adiabatic descent. A comparison of synthetic TOVS brightness temperatures with the observed HIRS2 12 radiance shows that rainfall assimilation reduces a moist UTH bias in the analysis in areas away from large precipitation changes. We interpret this drying to be associated with an enhanced subsidence in response to an improved latent heating field through rainfall assimilation. However, the synthetic radiance study also suggests that rainfall assimilation increases the bias and error std dev in UTH in areas of reduced precipitation, which is a direct consequence of the current moisture adjustment scheme depositing excessive moisture aloft. This procedure can be improved by concentrating the moisture adjustment in the lower troposphere. But a better long-term solution is to combine the rainfall and TPW assimilation procedure with TOVS moisture assimilation. Since the TOVS IR moisture channels are sensitive to UTH, they are complementary to the SSM/I TPW retrieval, which is sensitive to the moisture content in the lower troposphere.

While precipitation and TPW assimilation significantly improves the time-averaged analysis, its impact on short-range forecast ranges from neutral to modest improvements. The 6-h O–F statistics for tropical precipitation against SSM/I observations show less than 7% error std dev reductions in the first 12 h, which is small compared with the 30%–40% reductions of the error std dev in the 6-h averaged and monthly mean assimilated precipitation. Although the O–F residual for precipitation averaged over the Tropics is small, rainfall assimilation further reduces the tropical-mean bias by about 40% in forecasts beyond the first day. Rainfall and TPW assimilation does not improve nor degrade the monthly mean 6-h O–F statistics for winds and the geopotential height against rawinsonde observations in the Tropics. But the corresponding 6-h O–F statistics for moisture suggest moistening in the middle and upper troposphere, consistent with the synthetic radiance analysis.

Ensemble 5-day forecasts show that rainfall and TPW assimilation can reduce the rms error in forecasts up to 4 days in the Tropics. Rainfall and TPW assimilation does not lead to improved short-term forecasts in the extratropics but it is equally significant that it does not degrade the forecast while improving the time-averaged assimilation fields.

This study shows that the 6-h average SSM/I-derived precipitation estimate, despite uncertainties in its intensity, provides valuable information on the spatial distribution of rainfall, which can be used to improve global analyses. Earlier studies by Krishnamurti (1984, 1991, 1993, 1994) on physical initialization have shown that satellite-derived rain rate can be used to improve nowcasting and 1-day forecasts, but the impact is sensitive to the retrieved rainfall intensity. Since physical initialization improves the analysis through an improved forecast, this sensitivity is potentially an issue in satellite data applications. An advantage of our 1+1D procedure is that it uses observations to constrain the fields throughout the assimilation cycle rather than just at the initial time. The scheme is therefore not sensitive to deficiencies in the model physics or retrieval algorithms.

In this work we have assumed that the observations are perfect relative to the model estimates and that there is no cross correlation between moisture and temperature. But the methodology developed in this study can be extended to incorporate estimates of observation and model errors for a multivariate 1+1D problem, as described in section 2b. Results presented in this study provide a useful baseline for evaluating the performance of error covariance models in optimizing the IAU parameter estimate. Moreover, we have shown that satellite-derived rainfall and TPW data are useful for correcting model physics and reducing systematic errors in the assimilation fields. It may be possible to use this information to identify or correct systematic errors in the assimilation system. The improvements shown here were obtained using observations from two SSM/I instruments. With the launch of the TRMM satellite, which adds yet another microwave instrument with improved resolution to the existing two DMSP SSM/I instruments, we are optimistic that rainfall and TPW assimilation will be even more effective in improving the quality of assimilated global datasets in the near future.

Acknowledgments. It is a pleasure to acknowledge the support of Drs. Kenneth Bergman, Ramesh Kakar, and Ghassem Asrar of NASA Headquarters through Grants 578-41-60-20, 461-57-37-20, and 148-67-07, and TRMM Grants 622-32-33 and 622-24-27. We are grateful to Dr. Joanne Simpson for her encouragement and Dr. Robert Harriss for his support during his tenure as the science director of NASA's Mission to Planet Earth. We would also like to thank Genia Brin and Dennis Bungato for assistance in obtaining the 5-day forecast statistics, Dr. Man-Li Wu for a gridded version of Pinker's surface radiation data, Dr. William Olson for in-

formation on error estimates of GPROF retrievals, and Dr. Tadashi Tsuyuki for helpful comments on the manuscript.

REFERENCES

Adler, R., C. Kidd, M. Goodman, A. Ritchie, R. Schudalla, G. Petty, M. Morrissey, and S. Greene, 1996: PIP-3 intercomparison results. Report of the PIP-3 Workshop, College Park, MD. [Available online at http://www.ghcc.msfc.nasa.gov/pip3.]

Bell, T. L., A. Abdullah, R. L. Martin, and G. R. North, 1990: Sampling errors for satellite-derived tropical rainfall: Monte Carlo study using a space–time stochastic model. *J. Geophys. Res.*, **95,** 2195–2205.

Bloom, S. C., L. L. Takacs, A. M. da Silva, and D. V. Ledvina, 1996: Data assimilation using incremental analysis updates. *Mon. Wea. Rev.*, **124,** 1256–1271.

Caplan, P. M., G. H. White, and J. G. Jing, 1993: Skill of the NMC global model in the tropics. Preprints, *13th Conf. on Weather Analysis and Forecasting*, Vienna, VA, Amer. Meteor. Soc., 225–228.

Cohn, S. E., 1997: Introduction to estimation theory. *J. Meteor. Soc. Japan*, **75,** 257–288.

——, A. M. da Silva, J. Guo, M. Sienkiewicz, and D. Limbic, 1998: Assessing the effects of data selection with the DAO Physical-Space Statistical Analysis System. *Mon. Wea. Rev.*, **126,** 2913–2926.

DAO, 1996: Algorithm theoretical basis document, version 1.01. Data Assimilation Office, NASA/Goddard Space Flight Center. [Available online at http://dao.gsfc.nasa.gov/subpages/atbd.html.]

Dee, D. P., and A. M. da Silva, 1999: Maximum-likelihood estimation of forecast and observation error covariance parameters. Part I: Methodology. *Mon. Wea. Rev.*, **127,** 1822–1834.

——, G. Gaspari, C. Redder, L. Rukhovets, and A. M. da Silva, 1999: Maximum-likelihood estimation of forecast and observation error covariance parameters. Part II: Applications. *Mon. Wea. Rev.*, **127,** 1835–1849.

Derber, J. C., 1989: A variational continuous assimilation technique. *Mon. Wea. Rev.*, **117,** 2437–2446.

Donner, L. J., 1988: An initialization for cumulus convection in numerical weather prediction models. *Mon. Wea. Rev.*, **116,** 377–385.

Errico, R. M., and K. D. Raeder, 1999: An examination of the accuracy of the linearization of a mesoscale model with moist physics. *Quart. J. Roy. Meteor. Soc.*, **125,** 169–195.

Fillion, L., and R. Errico, 1997: Variational assimilation of precipitation data using moist convective parameterization schemes: A 1D-var study. *Mon. Wea. Rev.*, **125,** 2917–2942.

Fiorino, M., S. Lord, K.-M. Lau, P. A. Phoebus, and C. G. Strey, 1993: A synoptic-scale overview of the TOGA COARE International Observing Period November 1992–February 1993 based on analyses from U.S. operational global data assimilation systems. NASA Tech. Memo. 104593, 288 pp. [Available from NASA Goddard Space Flight Center, Greenbelt, MD 20771.]

Gruber, A., R. Ellingson, P. Ardanuy, M. Weiss, S. K. Uang, and S. N. Oh, 1994: A comparison of ERBE and AVHRR longwave flux estimates. *Bull. Amer. Meteor. Soc.*, **75,** 2115–2130.

Heckley, W. A, G. Kelly, and M. Tiedtke, 1990: On the use of satellite-derived heating rates for data assimilation within the tropics. *Mon. Wea. Rev.*, **118,** 1743–1757.

Huffman, G. J., 1997: Estimates of root-mean-square random error contained in finite sets of estimated precipitation. *J. Appl. Meteor.*, **36,** 1191–1201.

Illari, L., 1987: The ''spin-up'' problem. Tech. Memo. 137, ECMWF, Reading, United Kingdom, 27 pp.

Janowiak, J. E., 1992: Tropical rainfall: A comparison of satellite-derived rainfall estimates with model precipitation forecasts, climatologies, and observations. *Mon. Wea. Rev.*, **120,** 448–462.

Joiner, J., and A. M. da Silva, 1998: Efficient methods to assimilate remotely-sensed data based on information content. *Quart. J. Roy. Meteor. Soc.*, **124,** 1669–1694.

Kasahara, A., A. P. Mizzi, and L. J. Donner, 1994: Diabatic initialization for improvement in the tropical analysis of divergence and moisture using satellite radiometric imagery data. *Tellus*, **46A,** 242–264.

Krishnamurti, T. N., K. Ingles, S. Cocke, R. Pasch, and T. Kitade, 1984: Details of low latitude medium range numerical weather prediction using a global spectral model II. Effect of orography and physical initialization. *J. Meteor. Soc. Japan*, **62,** 613–649.

——, J. Xue, H. S. Bedi, K. Ingles, and O. Oosterhof, 1991: Physical initialization for numerical weather prediction over the tropics. *Tellus*, **43AB,** 53–81.

——, H. S. Bedi, and K. Ingles, 1993: Physical initialization using SSM/I rain rates. *Tellus*, **45A,** 247–269.

——, G. D. Rohaly, and H. S. Bedi, 1994: On the improvement of precipitation forecast skill from physical initialization. *Tellus*, **46A,** 598–614.

Kummerow, C., W. Olson, and L. Giglio, 1996: A simplified scheme for obtaining precipitation and vertical hydrometeor profiles from passive microwave sensors. *IEEE Trans. Geosci. Remote Sens.*, **34,** 1213–1232.

Ledvina, D. V., and J. Pfaendtner, 1995: Inclusion of Special Sensor Microwave/Imager (SSM/I) total precipitable water estimates into the GEOS-1 Data Assimilation System. *Mon. Wea. Rev.*, **123,** 3003–3015.

Manobianco, J., S. Koch, V. M. Karyampudi, and A. J. Negri, 1994: The impact of assimilating satellite-derived precipitation rates on numerical simulations of the ERICA IOP 4 cyclone. *Mon. Wea. Rev.*, **122,** 341–365.

Mathur, M. B., H. S. Bedi, T. N. Krishnamurti, M. Kanamitsu, and J. S. Woolen, 1992: Use of satellite derived rainfall for improving tropical forecasts. *Mon. Wea. Rev.*, **120,** 2540–2560.

Moorthi, S., and M. J. Suarez, 1992: Relaxed Arakawa–Schubert: A parameterization of moist convection for general circulation models. *Mon. Wea. Rev.*, **120,** 978–1002.

Olson, W. S., C. D. Kummerow, G. M. Heymsfield, and L. Giglio, 1996: A method for combined passive–active microwave retrievals of cloud and precipitation profiles. *J. Appl. Meteor.*, **35,** 1763–1789.

Peng, M. S., and S. W. Chang, 1996: Impacts of SSM/I retrieved rainfall rates on numerical prediction of a tropical cyclone. *Mon. Wea. Rev.*, **124,** 1181–1198.

Pfaendtner, J., S. Bloom, D. Limbic, M. Seablom, M. Sienkiewicz, J. Stobie, and A. da Silva, 1995: Documentation of the Goddard Earth Observing System (GEOS) Data Assimilation System—Version 1. NASA Tech. Memo. 104606, Vol. 4, NASA Goddard Space Flight Center, Greenbelt, MD. [Available online at http://dao.gsfc.nasa.gov/subpages/tech-reports.html.]

Pinker, R. T., and I. Lazlo, 1992: Modeling of surface solar irradiance for satellite applications on a global scale. *J. Appl. Meteor.*, **31,** 194–211.

Press, W. H., S. Teukolsky, W. Vetterling, and B. Flannery, 1992: *Numerical Recipes*. Cambridge University Press, 963 pp.

Puri, K., and M. J. Miller, 1990: The use of satellite data in the specification of convective heating for diabatic initialization and moisture adjustment in numerical weather prediction models. *Mon. Wea. Rev.*, **118,** 67–93.

Schubert, S. D., J. Pfaendtner, and R. Rood, 1993: An assimilated data set for earth science applications. *Bull. Amer. Meteor. Soc.*, **74,** 2331–2342.

Sienkiewicz, M., 1996: The GLA TOVS Rapid Algorithm forward radiance modules and Jacobian, version 1.0. DAO Office Note 96-08, Data Assimilation Office, Goddard Space Flight Center, Greenbelt, MD, 115 pp. [Available online at http://dao.gsfc.nasa.gov/subpages/office-notes#96-08.]

Smith, E. A., and Coauthors, 1998: Results of WetNet PIP-2 project. *J. Atmos. Sci.*, **55,** 1483–1536.

Susskind, J., J. Rosenfield, and D. Reuter, 1983: An accurate radiative transfer model for use in the direct physical inversion of HIRS

and MSU temperature sounding data. *J. Geophys. Res.,* **88,** 8550–8568.

——, ——, ——, and M. T. Chahine, 1984: Remote sensing of weather and climate parameters from HIRS2/MSU on TIROS-N. *J. Geophys. Res.,* **89,** 4677–4697.

——, P. Piraino, L. Rokke, L. Iredell, and A. Mehta, 1997: Characteristics of the TOVS Pathfinder Path A data set. *Bull. Amer. Meteor. Soc.,* **78,** 1449–1472.

Treadon, R. E., 1996: Physical initialization in the NMC global data assimilation system. *Meteor. Atmos. Phys.,* **60,** 57–86.

——, 1997: Assimilation of satellite derived precipitation estimates within the NCEP GDAS. Ph.D thesis, The Florida State University, Tallahassee, FL, 348 pp. [Available from Department of Meteorology, The Florida State University, Tallahassee, FL 32306.]

Trenberth, K. E., and J. G. Olson, 1988: An evaluation and intercomparison of global analyses from the National Meteorological Center and the European Centre for Medium Range Weather Forecasts. *Bull. Amer. Meteor. Soc.,* **69,** 1047–1057.

TRMM, 1996: Scientific operations plan. NASA/Goddard Space Flight Center, Greenbelt, MD, 122 pp. [Available online at http://trmm.gsfc.nasa.gov.]

Tsuyuki, T., 1996a: Variational data assimilation in the tropics using precipitation data. Part I: Column model. *Meteor. Atmos. Phys.,* **60,** 87–104.

——, 1996b: Variational data assimilation in the Tropics using precipitation data. Part II: 3D model. *Mon. Wea. Rev.,* **124,** 2545–2561.

——, 1997: Variational data assimilation in the Tropics using precipitation data. Part III: Assimilation of SSM/I precipitation rates. *Mon. Wea. Rev.,* **125,** 1447–1464.

Turpeinen, O. M., L. Garand, R. Benoit, and M. Roch, 1990: Diabatic initialization of the Canadian Regional Finite-Element (RFE) model using satellite data. Part I: Methodology and application to a winter storm. *Mon. Wea. Rev.,* **118,** 1381–1395.

van Tuyl, A. H., 1996: Physical initialization with the Arakawa–Schubert scheme in the navy's operations global forecast model. *Meteor. Atmos. Phys.,* **60,** 47–55.

Vukicevic, T., and R. M. Errico, 1993: Linearization and adjoint of parameterized moist diabatic processes. *Tellus,* **45A,** 493–510.

WCRP, 1998: *Proceedings of the First WCRP International Conference on Reanalyses.* World Climate Research Program, 461 pp.

Wentz, F. J., 1994: Users' manual: SSM/I-2 geophysical tapes. Remote Sensing Systems, Santa Rosa, CA, 11 pp. [Available online at http://www.ssmi.com.]

——, 1997: A well calibrated ocean algorithm for SSM/I. *J. Geophys. Res.,* **102** (C4), 8703–8718.

White, G. H., E. Kalnay, R. Gardner, and M. Kanamitsu, 1993: The skill of precipitation and surface temperature forecasts by the NMC global model during DERF II. *Mon. Wea. Rev.,* **121,** 805–814.

Zupanski, D., 1993: The effects of discontinuities in the Betts–Miller cumulus convection scheme on four-dimensional variational data assimilation. *Tellus,* **45A,** 511–524.

——, 1997: A general weak constraint applicable to operational 4DVAR data assimilation systems. *Mon. Wea. Rev.,* **125,** 2274–2292.

——, and F. Mesinger, 1995: Four-dimensional variational assimilation of precipitation data. *Mon. Wea. Rev.,* **123,** 1112–1127.

Zupanski, M., 1993: Regional four-dimensional variational data assimilation in a quasi-operational forecasting environment. *Mon. Wea. Rev.,* **121,** 2396–2408.